Geobiology (2008), **6**, 481–502 DOI: 10.1111/j.1472-4669.2008.00179.x

In-situ grown silica sinters in Icelandic geothermal areas

DOMINIQUE J. TOBLER[1], ANDRI STEFÁNSSON[2] AND LIANE G. BENNING[1]

[1]*Earth and Biosphere Institute, School of Earth and Environment, University of Leeds, LS2 9JT, UK*
[2]*Institute of Earth Sciences, University of Iceland, Sturlugata 7, 101 Reykjavík, Iceland*

ABSTRACT

Field *in-situ* sinter growth studies have been carried out in five geochemically very different Icelandic geothermal areas with the aim to quantify the effects of water chemistry, (e.g. silica content (250 to 695 p.p.m. SiO_2), salinity (meteoric to seawater), pH (7.5 to 10)), temperature (42–96 °C) and microbial abundance (prevalence, density) on the growth rates, textures and structures of sinters forming within and around geothermal waters. At each location, sinter growth was monitored over time periods between 30 min and 25 months using glass slides that acted as precipitation substrates from which sinter growth rates were derived.

In geothermal areas like Svartsengi and Reykjanes, subaqueous sinters developed rapidly with growth rates of 10 and 304 kg $year^{-1}$ m^{-2}, respectively, and this was attributed primarily to the near neutral pH, high salinity and medium to high silica content within these geothermal waters. The porous and homogeneous precipitates that formed at these sites were dominated by aggregates of amorphous silica and they contained few if any microorganisms. At Hveragerdi and Geysir, the geothermal waters were characterized by slightly alkaline pH, low salinity and moderate silica contents, resulting in substantially lower rates of sinter growth (0.2–1.4 kg $year^{-1}$ m^{-2}). At these sites sinter formation was restricted to the vicinity of the air–water interface (AWI) where evaporation and condensation processes predominated, with sinter textures being governed by the formation of dense and heterogeneous crusts with well-defined spicules and silica terraces. In contrast, the subaqueous sinters at these sites were characterized by extensive biofilms, which, with time, became fully silicified and thus well preserved within the sinter edifices. Finally, at Krafla, the geothermal waters exhibited high sinter growth rates (19.5 kg $year^{-1}$ m^{-2}) despite being considerably undersaturated with respect to amorphous silica. However, the bulk of the sinter textures and structure were made up of thick silicified biofilms and this indicated that silica precipitation, i.e. sinter growth, was aided by the surfaces provided by the thick biofilms. These results further suggest that the interplay between purely abiotic processes and the ubiquitous presence of mesophilic and thermophilic microorganisms in modern silica rich terrestrial hydrothermal settings provides an excellent analogue for processes in Earth's and possibly Mars's ancient past.

Received 4 July 2008; accepted 10 October 2008

Correspondence: Dominique J. Tobler. Tel.: (+44) 113 343 5220; fax: (+44) 113 343 5259; e-mail: tobler@see.leeds.ac.uk

INTRODUCTION

Iceland is well known for its geothermal areas that are the surface expression of the narrow belt of active faulting and volcanism caused by the Mid-Atlantic Ridge and the Greenland–Iceland–Faeroes Ridge. The geothermal areas include features such as mudpots, geysers, fumaroles and hot springs, most of which are inhabited by diverse mesophilic and thermophilic microbial life. In addition, outflow waters and condensed steam from wells and geothermal power stations created various man-made features, i.e. channels and pools (e.g. Blue Lagoon). The precipitation of silica in these systems is a well-known process leading to the formation of silica sinters (e.g. Arnórsson, 1975) and the full silicification and subsequent fossilization of microorganisms (e.g. Schultze-Lam *et al.*, 1995; Konhauser *et al.*, 2001). These microfossils are preserved in modern silica sinters and thus provide a modern analogue to fossilization in ancient siliceous terrestrial environments (Cady & Farmer, 1996; Konhauser & Ferris, 1996) and may even be important for our understanding of the silica sinter deposits postulated to exist on Martian surface (Ruff *et al.*, 2007; Squyres *et al.*, 2008).

Laboratory experiments and studies on natural geothermal environments (e.g. Taupo Volcanic Zone, New Zealand; Yellowstone, USA) suggest that the mechanisms triggering silica precipitation, i.e. sinter growth, are purely abiotic (e.g. Walter *et al.*, 1972; Mountain *et al.*, 2003 and references therein) and that silica saturation and precipitation are mostly induced by rapid cooling and boiling of geothermal waters or by co-precipitation with auxiliary minerals (e.g. Guidry & Chafetz, 2003; Mountain *et al.*, 2003). Cooling seems to be the predominant process controlling the deposition of subaqueous sinter within geothermal systems. However, many silica sinters encountered in thermal hot spring areas are often formed subaerially (at or above the air–water interface, AWI) and for their formation, other hydrodynamic processes including wave action, capillary action, diffusion and splash must also be invoked (e.g. Mountain *et al.*, 2003 and references therein).

In most geothermal areas microorganisms are ubiquitous and variations in silicification textures and structures of microbial communities have received considerable attention over the last four decades (e.g. Walter *et al.*, 1972; Ferris *et al.*, 1986; Schultze-Lam *et al.*, 1995; Cady & Farmer, 1996; Hinman & Lindstrom, 1996; Konhauser & Ferris, 1996; Renault *et al.*, 1996; Jones *et al.*, 1997, 1998; Phoenix, 2001; Konhauser *et al.*, 2001; Mountain *et al.*, 2003; Jones *et al.*, 2004; Lalonde *et al.*, 2005). These studies all concluded that microorganisms played only an indirect role in the silicification process as there are no metabolic advantages to microbial silicification. However, these studies also showed that the microbial surfaces (e.g. cell walls, extracellular polysaccharides) provide suitable sites for the adhesion of silica particles formed in solution and thus they allow different sinter textures and structures (governed by microbial cell morphology, e.g. filaments, bacillus, cocci) to develop.

Despite these efforts, the relationships between the geochemical parameters (that govern sinter growth rates) and the sinter fabrics as well as the associated microbiology are still poorly understood mostly due to a dearth of quantitative and *in-situ* labratory and field analyses. Only few studies (e.g. Jones *et al.*, 1999, 2004; Konhauser *et al.*, 2001; McKenzie *et al.*, 2001; Mountain *et al.*, 2003; Smith *et al.*, 2003; Handley *et al.*, 2005; Schinteie *et al.*, 2007) determined sinter growth rates using artificial substrates and among them even fewer (Mountain *et al.*, 2003; Smith *et al.*, 2003 and Handley *et al.*, 2005) monitored growth rates on silica slides over long timescales and characterized the structure and texture of the forming sinters at periodic time steps. Such *in-situ* field studies of sinter growth were mostly done in geothermal areas in New Zealand (e.g. Mountain *et al.*, 2003; Handley *et al.*, 2005) and they showed that at high sinter growth rates (≥ 2 mg slide^{-1} day^{-1}; Handley *et al.*, 2005) the sinter fabric on the slides were governed primarily by the physico-chemical characteristics of the geothermal waters (e.g. Mountain *et al.*, 2003; Handley *et al.*, 2005); in the vicinity of the AWI, where evaporation and cooling processes dominate, the sinter textures were dense and mostly made up of fine granular silica layers, whereas in the submerged parts of the slides, porous-granular sinter deposits formed due to the prolonged period of silica polymerization. At moderate to low deposition rates (i.e. in less saturated waters), extensive microbial mats developed and the slow but continuous deposition of newly formed silica nanospheres onto the microbial surfaces eventually led to their complete silicification and preservation within the sinter edifice (e.g. Walter *et al.*, 1972; Ferris *et al.*, 1986; Schultze-Lam *et al.*, 1995; Cady & Farmer, 1996; Konhauser & Ferris, 1996; Jones *et al.*, 1998; Konhauser *et al.*, 2001; Mountain *et al.*, 2003). Close to the AWI, spicular sinters and silica terraces may form (subaerially), whereas porous-filamentous or flat, laminated silica crusts dominate the subaqueous parts of the slides (e.g. Mountain *et al.*, 2003; Handley *et al.*, 2005).

In Iceland, most studies related to silica sinter formation focussed either on the characterization of sinters and the impact of microbes on the sinter structures and textures (Schultze-Lam *et al.*, 1995; Konhauser & Ferris, 1996; Konhauser *et al.*, 2001), or on the analysis of specific microbial assemblages and diversities in these waters (e.g. Pétursdóttir & Kristjánsson, 1996; Sonne-Hansen & Ahring, 1997; Chung *et al.*, 2000; Skírnisdóttir *et al.*, 2000; Hjorleifsdottir *et al.*, 2001; Kvist *et al.*, 2007), or on silica scaling in geothermal power developments (e.g. Kristmannsdóttir, 1989; Thordarson & Tómasson, 1989; Gunnarsson & Arnórsson, 2003). However, there is as yet no comparative, combined geochemical and structural study of the formation and growth rates of silica sinters in Icelandic geothermal waters.

To overcome this gap, in this study, *in-situ* sinter growth experiments were carried out in five different Icelandic geothermal areas (Fig. 1) with the main aim to quantify how variations in geochemical parameters (e.g. pH, temperature, salinity, silica concentration) and the abundance of microorganisms affected the growth rates and the textures and structures of the formed sinters. At each location, the *in-situ* growth of silica sinters were quantified based on precipitates that formed on glass slides and the resulting sinter deposits were characterized using spectroscopic and microscopic methods. The data were compared to results from other *in-situ* field studies on sinter growth.

METHODS

Sampling protocols

In September 2005 short- and long-term *in-situ* sinter growth experiments were set up in five geothermal areas in Iceland including Geysir, Hveragerdi, Reykjanes, Svartsengi and Krafla (Fig. 1). Prior to each sinter growth experiment, the temperature and pH of the geothermal waters were determined *in-situ* using a KT-thermocouple (±0.2) and a Hanna pH meter (±0.05, calibrated at temperature). The water flow rates were determined at each site by measuring the time for a floating object (e.g. leaves, paper) to pass a

Fig. 1 Map of sampling locations in Iceland where *in-situ* sinter growth experiments were carried out.

certain distance (usually at least 2–7 m). Subsequently, 150 mL samples of spring or drain water were filtered through a sterile single-use 0.2 μm polycarbonate filter unit for cation (acidified on site with concentrated HNO_3, ratio 1 : 50) and for anion (non-acidified) determination. Additionally, 50 mL were filtered through the 0.2 μm polycarbonate filter unit for total silica (concentrated NaOH added on site, 1 : 10 ratio) analysis. All solution samples were stored in the fridge at ~4 °C.

At each site a Teflon tray holding 20 microscope glass slides (four rows with five 25 × 75 mm slides) was immersed into the geothermal water either within an outflow channel or close to a pool rim. The tray was placed in such a way that the top section of each slide (maximum 1 cm) was partially exposed to air. Over a time period between 30 min and 25 months, sets of five slides were collected at specific time intervals and analysed.

Immediately after removal from the trays, individual slides were transferred into sterile 50 mL tubes and subsequently stored in the fridge at ~4 °C. Three out of five collected slides (at each sampling step) were used to determine precipitation rates after drying in an oven at 60 °C and weighing. The difference in weight between sinter covered and uncovered slides provided an average silica precipitation rate and standard deviation in kilograms of precipitate per year and per square metre. The remaining two slides were fixed in the field with filtered 2.5% glutaraldehyde solutions and used for the characterization of microbial cell morphologies. Upon return to the laboratory the glutaraldehyde-fixed slides were washed once with a phosphate buffer (pH = 7) and then stepwise dehydrated using a series of ethanol exchange steps (30, 50, 70, 90, 100%). In addition, at Reykjanes and Svartsengi, the sterile filters used for the water collection were preserved and the untreated filters were analysed for particulates.

Solution analyses

Cations were measured by inductively coupled plasma optical emission spectrometer (ICP-OES) using a Thermo Jarell Ash IRIS spectrometer and anions were determined using a Dionex DX-600 ion chromatograph (IC) using an IonPac AS16 column and a KOH eluent. Total silica (monomeric plus polymeric fraction) was analysed with the spectrophotometric molybdate yellow method (Greenberg *et al.*, 1985).

To calculate the saturation state of silica within each geothermal system studied, the major chemical constituents (Table 1), temperature and pH (mean T and pH values were used where T and pH fluctuated over the time period studied) of the geothermal waters were used as inputs for geochemical modelling using the geochemical code PHREEQC (version 2.13.3; Parkhurst & Appelo, 1999) and the wateq4 database (Ball & Nordstrom, 1992) with the amorphous silica data updated using the values from Gunnarsson & Arnórsson (2000). Saturation indices, $SI = \log (IAP/K_{sp})$, were calculated for each geothermal system, with IAP being the ionic activity product and K_{sp} the solubility product and where $SI > 0$ represents supersaturation and $SI < 0$ undersaturation.

Solids analyses

For microscopic imaging and qualitative elemental analyses, slides or filters were dried and placed on a sticky carbon pad covering an aluminium stub, then coated with a 3-nm platinum layer and analysed using a Field Emission Gun Scanning Electron Microscope (FEG-SEM, LEO 1530) equipped with an Oxford Instruments energy dispersive X-ray (EDX) detector and INCA software. Images were collected at 3 kV and a

Table 1 Chemical composition of geothermal waters in which *in-situ* experiments were conducted

	Krafla wastewater drain	GY1 Upper spring	GY2* Sodi spring	Hveragerdi wastewater drain	Svartsengi wastewater drain		Reykjanes wastewater drain
Date	22/9/05	20/9/05	20/9/05	25/9/05	21/9/05		21/9/05
pH/°C	9.95/50	8.47/48	8.45/43	9.05/55	7.74/41.9		7.50/39.8
T (°C)	80	70–96†	82	66	42		75
Flow rate (m/s)	0.44	up to 0.5†	0.25	0.42	–‡		–§
p.p.m							
Al	1.72	0.52	0.23	0.74	2.00		<0.1
B	0.98	0.79	1.00	0.42	6.01		5.49
Ca	3.85	1.12	1.34	3.26	1332		2550
Fe	0.08	0.09	0.12	0.05	2.80		5.90
K	39	11	13	13	1316		2314
Li	0.27	0.24	0.27	0.07	3.81		7.67
Mg	0.03	0.01	0.07	0.11	0.62		0.71
Mn	<0.005	<0.005	<0.005	<0.005	0.22		2.01
Na	269	234	242	168	8067		14 657
SiO_2¶	603	363	372	304	250**		695
Sr	<0.1	< 0.1	< 0.1	< 0.1	9.0		9.4
Cl	74	114	117	120	14 854		27 174
F	2.08	20	15	3.24	<0.2		<0.2
NO_3	<0.2	<0.2	<0.2	0.76	23		43
SO_4	262	91	107	60	30		18
Slide collection**	25 months	5 d	= GY1	3 months	1st	2nd	0.5 h
		3 months	(both	5 months	3 h	4 d	1 h
		5 months	GY2 and 3)	8 months	6 h	7 d	2 h
		8 months		13 months	19 h	11 d	3 h
					24 h	17 d	5 h
					5 d		7.5 h

*Water chemistry at GY3 (T = 61 °C) was assumed to be identical to GY2 due to their proximity (~10 m).
†Temperature and flow rate fluctuated due to frequent surges.
‡Wastewater pool where water flow was minor and wave action predominated.
§Water flow rate could not be determined.
¶Total SiO_2 was measured from filtered water samples to which base was added.
**d: days, h: hours.

working distance of 4 mm, while for EDX analysis the working distance was increased to 8 mm and the accelerating voltage to 15 kV. The size distributions of the silica particles on the slides from Svartsengi and Reykjanes were determined from the recorded SEM photomicrographs. To obtain a size distribution with reasonably high precision, 140 particles were measured for both sites and the mean values and standard deviations were calculated.

The mineralogical composition of the fresh precipitates formed on the slides at each sampling site was analysed using X-ray powder diffraction (XRD). About 200 mg of precipitate was carefully scraped off an unfixed glass slide, the material was dried and ground to a fine powder and deposited on a silicon sample holder. Analyses were carried out with a Philips PW1050 diffractometer, and scans were acquired from 5 to 70°2θ at 1°/min with a step size of 0.02° and operating conditions of 40 kV and 30mA using CuKα radiation. Data were analysed and compared to published data for standard minerals in the JCPDF files (International Center for Diffraction Data®, Newtown Square, PA, USA).

RESULTS

Geysir geothermal area

The Geysir geothermal area is situated on the Southern Lowlands (Fig. 1) at an elevation of about 120 m. The geothermal activity is characterized by hot springs and geysers ranging from <20 °C to 100 °C. The main geothermal activity occurs within an area of only a few hundred metres across, but thermal manifestations are spread over an area of approximately 3 km^2. The waters at Geysir geothermal field are meteoric of origin (Table 1) and are characterized by low abundance of dissolved solids (<150 p.p.m. Cl), with Si, Na, Cl and SO_4 being the dominant dissolved elements. Based on chemical geothermometry, the underground aquifer temperatures are >250 °C and the composition with respect to major elements is considered to be controlled by equilibrium with mineral-buffer reactions at the aquifer temperature or in the upflow zone with rhyolitic and basaltic rocks (Arnórsson, 1985).

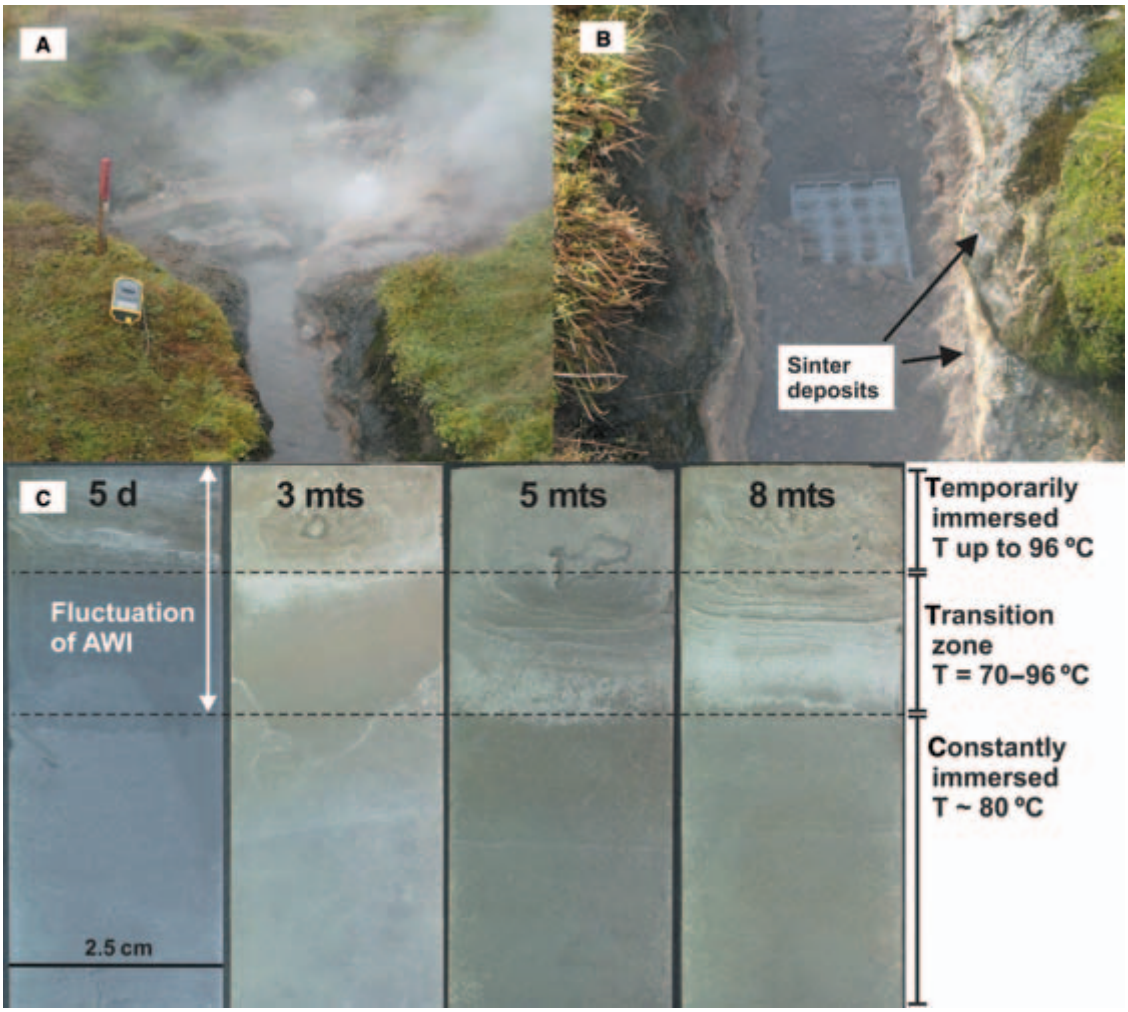

Fig. 2 (A) Spring and outflow channel of GY1. (B) Close-up of sampling tray. (C) Glass slides collected at GY1 with typical increase in silica deposits for time periods between 5 days and 8 months (mts). AWI, air–water interface.

Two different thermal features were chosen for sinter growth studies at Geysir: upper spring (thereafter called GY1, Fig. 2A), representing the outflow from an old borehole, and Sodi spring (Fig. 3A), a natural thermal spring where two different temperature regimes were studied (thereafter called GY2 and GY3, Fig. 3B,C). At both Geysir sites, the moderately high total silica contents (363 and 372 p.p.m. SiO_2 at GY1 and GY2, respectively) and the hard and compact sinter deposits that formed within and along the outflow channels (Figs 2B and 3B) indicated relatively low precipitation rates. XRD analyses of the newly formed sinters showed opal-A (i.e. amorphous silica) as the sole precipitating phase (Fig. 4; GY1-3 patterns).

Upper spring (GY1)

Sampling and sinter growth experiments were carried out in the outflow channel of GY1 (Fig. 2B) at an average water temperature of 80 °C and at pH 8.47 (at 48 °C). This site was characterized by frequent violent surges (every 1–2 min) which affected the temperature, the flow rates and the level of immersion of the slides (Fig. 2C). As a result, the temperatures measured at the AWI fluctuated between 70 and 96 °C, the flow rate varied between 0 and 0.5 m s^{-1} and the slides were occasionally fully submerged. From the slides collected over a time period of 8 months (Table 1, Fig. 2C), an average silica precipitation rate of 0.2 ± 0.1 kg $year^{-1}$ m^{-2} was derived.

FEG-SEM examinations of the slides collected after 5 days (Fig. 5) showed an extremely heterogeneous texture of the precipitates that consisted of a combination of amorphous silica and various microbial cell morphologies. The top sections of the slides, occasionally fully submerged (due to the frequent surges), were dominated by dense silica layers and spicular structures (Fig. 5A). These dense layers consisted of silica nanoparticles that coalesced into

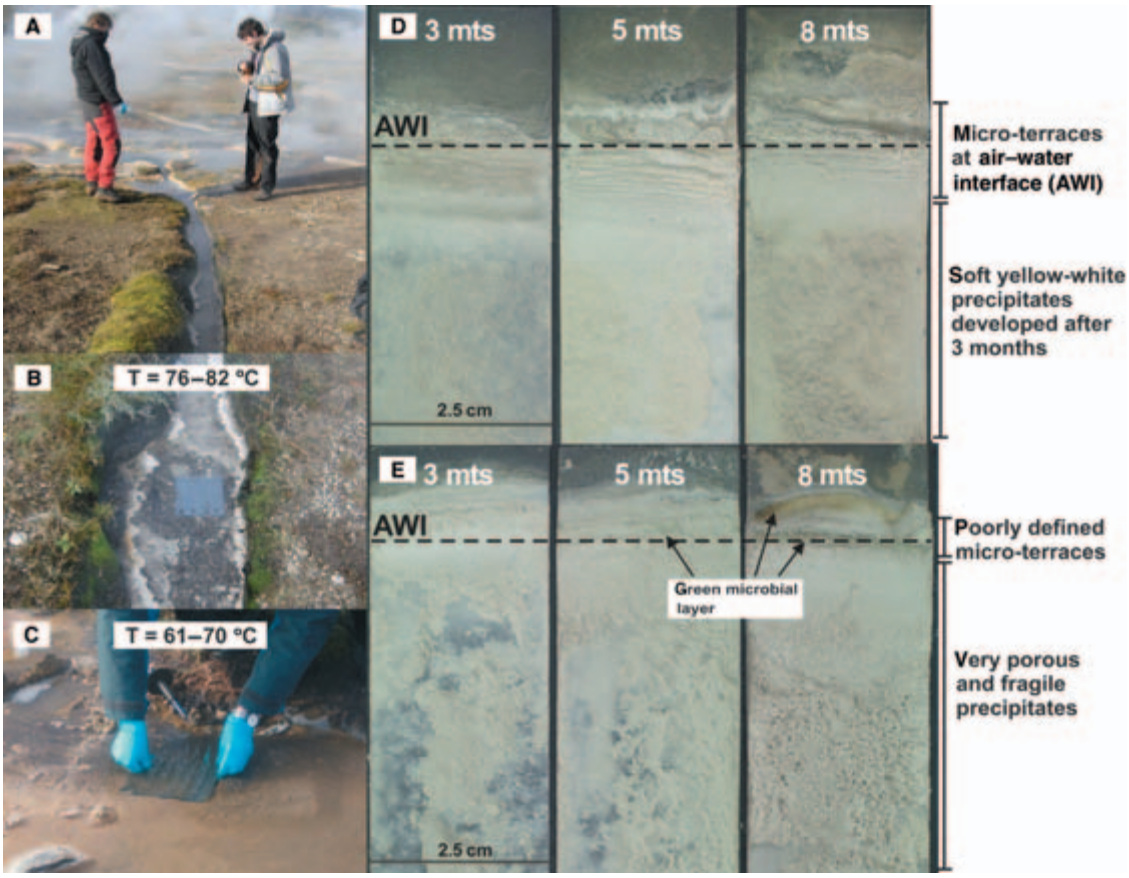

Fig. 3 (A) Spring and outflow channel of Sodi spring, (B and C) position of sampling trays at GY2 and GY3, respectively, (D and E) slides collected from the tray placed at GY2 and GY3, respectively, for a time period between 3 and 8 months (mts).

smooth films and formed at the AWI presumably due to fast evaporation and cooling. The spicules (defined as vertical columnar or domal structures; e.g. Handley *et al.*, 2005 and references therein) consisted primarily of alternating layers of silica and microorganisms (Fig. 5B). Although microorganisms were present in these upper zones, the significant temperature fluctuations were less favourable for the growth and stability of large microbial communities and the colonization was sparse. Further down the slides, a transition zone (temporarily above the AWI, Fig. 2C) with no spicules, more heterogeneous silica layers and greater quantities of microorganisms were observed. It is worth noting, that after 5 days, some microorganisms were already partly silicified. The bottom of the slides, which was permanently submerged (T ~ 80 °C), showed little silica deposition after 5 days but in all cases dense microbial biofilms were present. Overall, in this zone the microbes were mainly filamentous with a diameter of approximately 0.3 µm and a length ranging between 2 and 15 µm, interspersed with few rod-shaped microorganisms.

After 3 months, the slides were covered with considerably larger amounts of silica, yet the textural and structural characteristics of the precipitates were basically unchanged. However, rod-shaped bacteria as well as cocci had colonized the side of spicules (Fig. 5C). In the transition zone (Fig. 5D), a few filaments were possibly sporulating which might have been triggered by the harsh temperature variations induced by the frequent surges. The lower parts of the slides were still covered with dense microbial mats, but after 3 months, extensive silicification was observed (Fig. 5E).

Slides collected after 5 and 8 months showed almost identical features to those observed in the 3 months slides, the main difference being the amount of silica precipitated and the degree of silicification of the microorganisms (silicified both externally and internally, Fig. 5F).

Sodi spring (GY2 and GY3)

Sodi spring is located to the north-west of the main entrance to the Geysir geothermal area. Trays with glass slides were placed at two different sites within the outflow channel of Sodi spring. The first sampling site (GY2, Fig. 3B) was in an outflow channel ~5 m away from the emergence point of Sodi spring. The average water temperature was 79 °C, the pH was 8.45 (at 43 °C) and the flow rate was 0.25 m s^{-1}. The second tray (GY3, Fig. 3C) was placed in the same outflow channel but

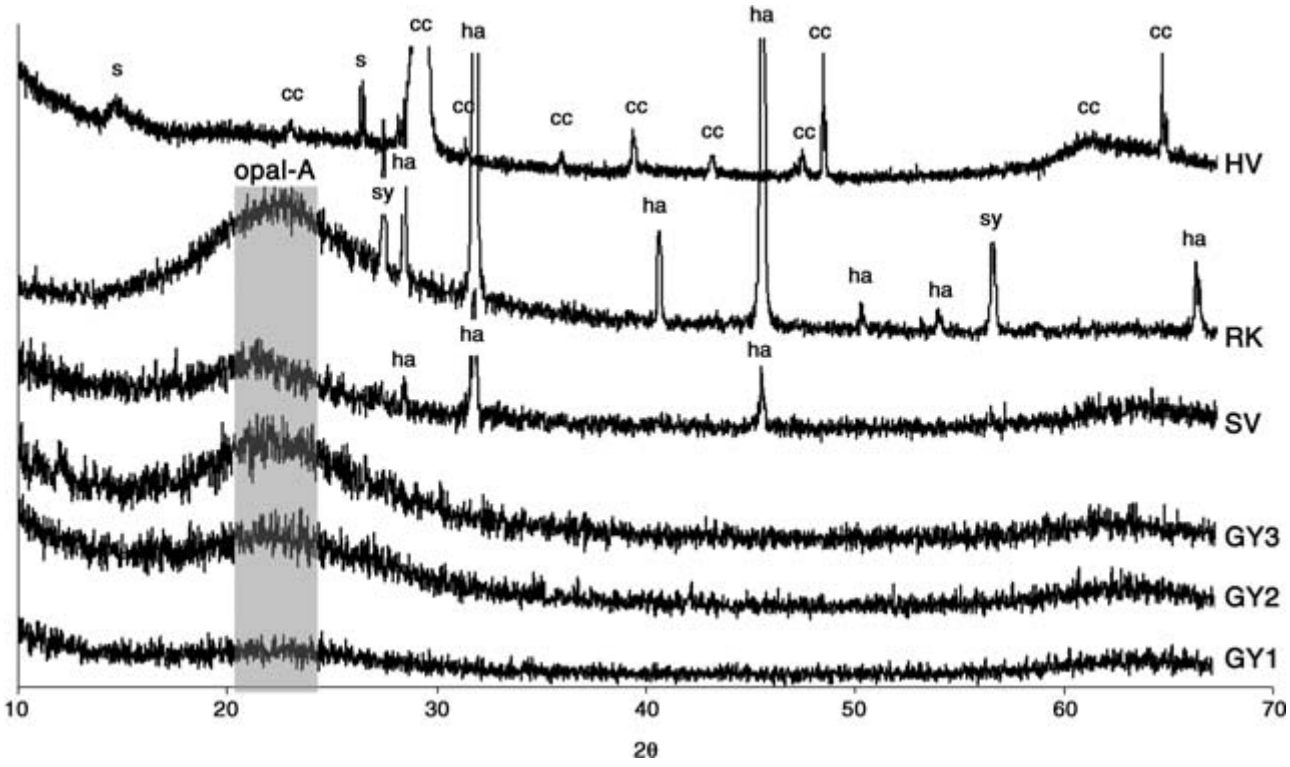

Fig. 4 X-ray powder diffraction pattern of precipitates from Hveragerdi (HV), Reykjanes (RK), Svartsengi (SV), and Geysir (GY1-3). Shaded area shows 2θ-range characteristic for the broad XRD peak of opal-A, i.e. amorphous silica (Herdianita *et al*., 2000). ha: halite, sy: sylvite, cc: calcite, s: sulfur.

about 15 m away from the spring where the average temperature was ~15 °C lower (T_{ave} = 65 °C). The goal of the two sets of experiments within the same outflow channel was to determine how sinter growth rates as well as microbial communities were affected by temperature while all other conditions were similar.

At both sites, slides were removed at specific times between 5 days and 8 months (Table 1, Fig. 3D,E) from which a silica precipitation rate of 0.7 ± 0.3 kg year^{-1} m^{-2} was estimated for GY2 and 1.4 ± 0.4 kg year^{-1} m^{-2} for GY3.

At GY2, after 5 days considerable amounts of silica precipitated as layers and terraces in the vicinity of the AWI but no spicules and only few microbes were observed. The few microorganisms present were mostly rod-shaped with lengths between 1.5 to 3 μm and an average width of 0.3 μm and with some already partly silicified after this short time (Fig. 6A). A bit further down the slides, long filaments became more abundant and they mainly covered small terraces that had formed between the various silica layers (Fig. 6B). In the subaqueous parts of the slides, dense biofilms consisting of very long and thin microbial filaments (width ~0.3 μm, 10–50 μm long) were observed (Fig. 6C) and hardly any silica precipitates were associated with these filamentous mats.

After 3 months, the appearance of the slides changed significantly with yellow-white precipitates covering about two thirds of the slides (Fig. 3D). In the vicinity of the AWI, distinct silica terraces (overall vertical height up to 1 mm, Fig. 3D) and spicule-like structures (Fig. 6D) developed as a consequence of evaporation and cooling. The textures of these terraces seemed very different compared to the small terraces observed after 5 days (Fig. 6B) and consisted of thin and dense layers of silica covering accumulations of partly to fully silicified microorganisms interspersed with silica aggregates (Fig. 6D). The heterogeneous, yellow-white precipitates covering the bottom part of the slides (Fig. 3D) consisted solely of a network of silicified as well as unsilicified filaments, free silica aggregates and a few diatoms. The diatoms interspersed with the silicified filaments, although not indigenous (water temperature was far too high for diatoms to survive; Brock, 1978), were probably blown into the spring as aerosols.

After 8 months, the silica terraces on the slides reached an overall height of up to 3 mm and far more precipitates were covering the slides; however, the structures and textures of the precipitates did not change significantly during the latter 5 months of growth.

At GY3, the slides were dominated by porous and fragile precipitates (Fig. 3E). The textures in the submerged parts of the slides were uniform regardless of the time interval at which they were collected and basically consisted of dense silica layers that alternated with porous, microbe-rich aggregates (Fig. 7A). Similar to GY2, these porous aggregates consisted of filamentous (both exhibiting various stages of silicification), free silica aggregates as well as a few diatoms (Fig. 7B). At the AWI, the

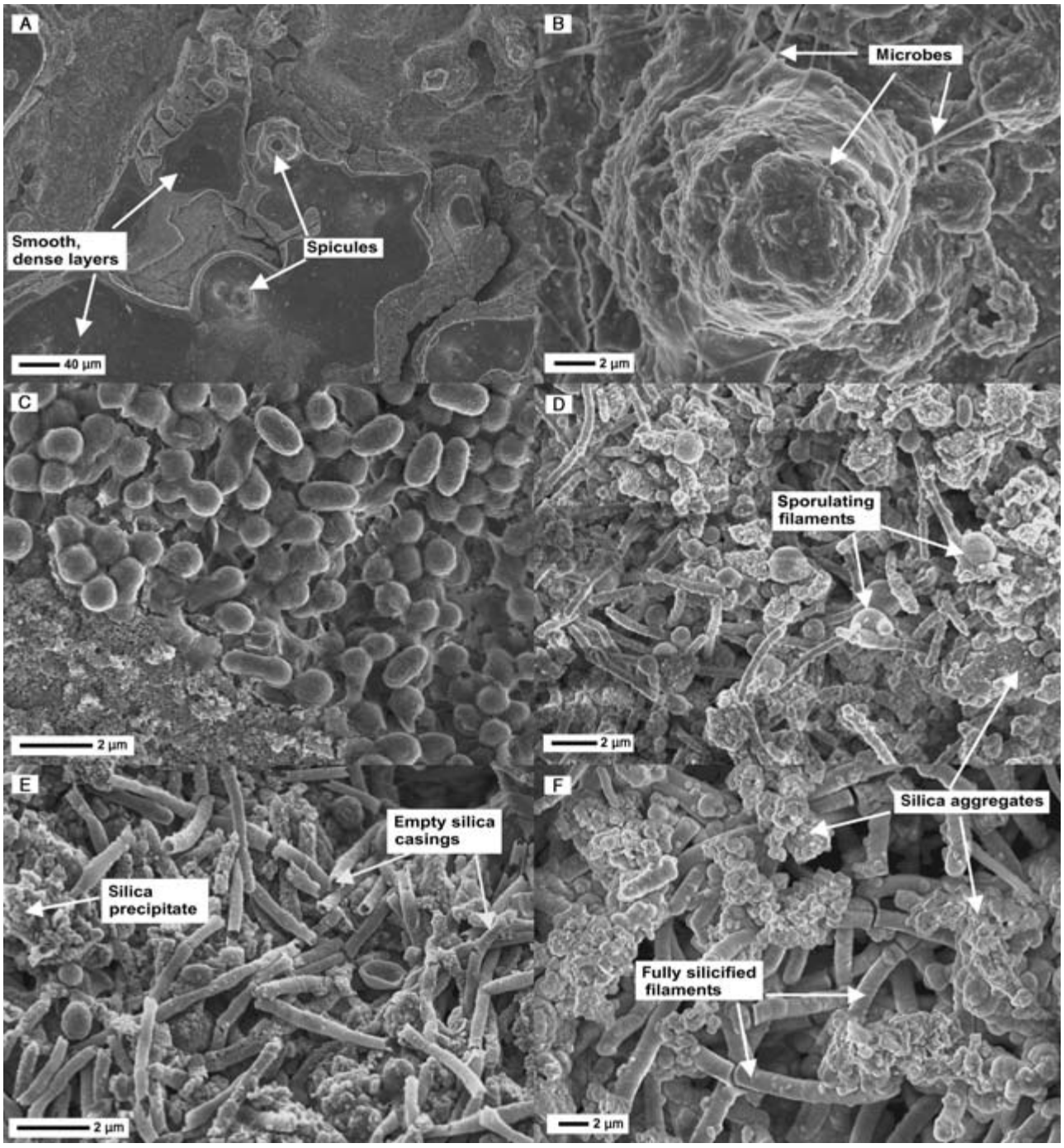

Fig. 5 Photomicrographs of slides collected at GY1 (A–B: after 5 days, C–E: after 3 months, F: after 8 months). (A) Multiple dense silica layers and spicules at the AWI. (B) Close-up of a single spicule. (C) Cocci and rod-shaped microbes found on the side of a spicule. (D) Microbial filaments, possibly sporulating, surrounded by silica aggregates from the transition zone. (E) Empty silica casings left behind by encrusted microbial filaments. (F) Mix of fully silicified microbial filaments and silica aggregates in the lower parts of the slides.

sinter fabrics consisted of silica spheres and biofilms cemented together in the form of thick layers (Fig. 7C) and no distinct silica terraces or spicules were observed. It is worth noting that after 5 months, a thin green layer developed at the AWI where the temperature was about 5 °C lower than within the constantly submerged part (Fig. 3E arrows). This green layer increased in thickness significantly over the following 3 months and its formation indicated the colonization of the sinter deposited

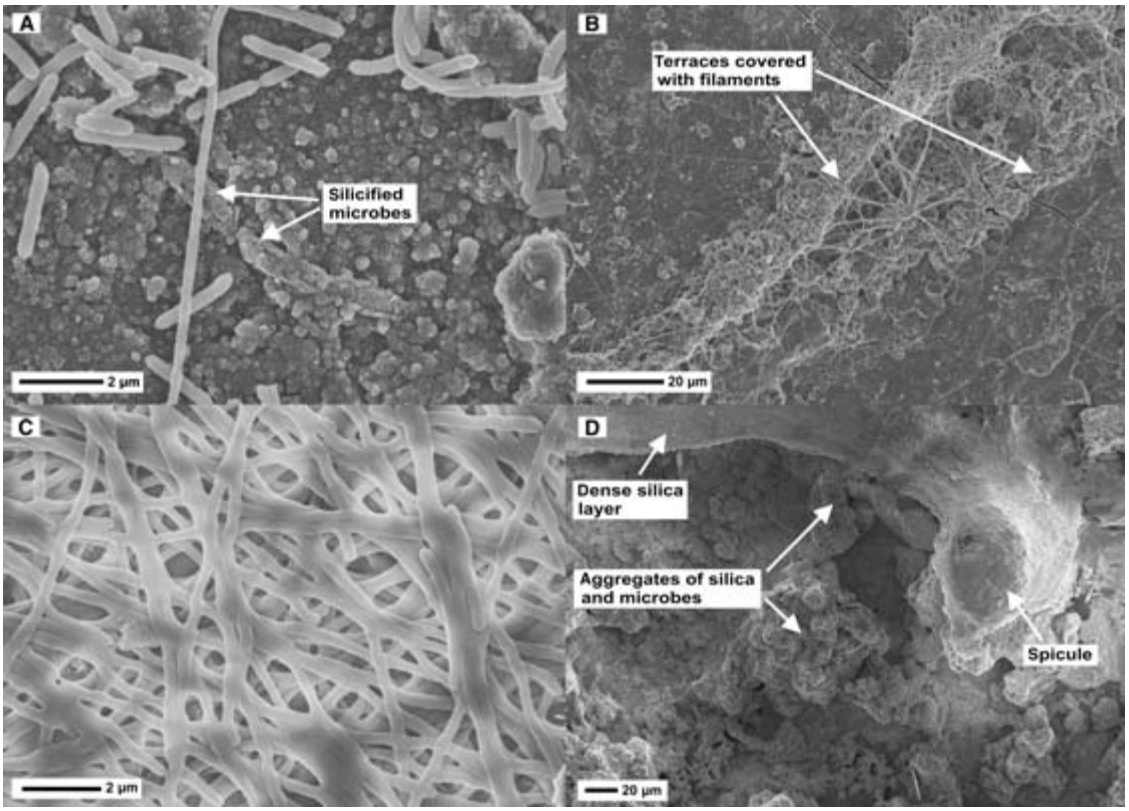

Fig. 6 Photomicrographs of slides collected from GY2 (A–C: after 5 days, d: after 3 months). (A) Unsilicified rod-shaped microorganisms, very thin and long microbial filaments as well as silicified microbes on dense silica substrate, precipitated in the vicinity of the air–water interface (AWI). (B) Terraces formed by silica layers densely populated by long, thin filaments from the middle part of the slides. (C) Dense unsilicified microbial biofilm from the fully submerged part of the slides. (D) Spicule-like structure surrounded by coarse and very porous aggregates consisting of silica and silicified microorganisms (at the AWI).

on or above the AWI with photosynthesizing microorganisms. Interestingly, in this green layer only large accumulations of partly to fully silicified filaments, interlinked and embedded in layers of blocky silica (Fig. 7A,B) were observed and these did not differ in textures and structures from the rest of the slide. At GY3, the silicification of microorganisms followed the same patterns as seen in the other two Geysir sites, with silica spheres adhering to the surface of microbial cells and at longer time scales fully covering and preserving them (Fig. 7D).

Hveragerdi wastewater drain (HV)

The Hveragerdi geothermal area is located on the Southern Lowlands, approximately 45 km east of the capital, Reykjavik. The area is characterized by hot springs ranging from <20 °C to 100 °C and steam fumaroles. Several drill holes that have been sunk into the area have shown deep aquifer temperatures up to 200 °C (Arnórsson *et al.*, 1983b). The waters at Hveragerdi geothermal field are of meteoric origin (Table 1) and their chemistry is considered to be controlled by basalt–water interaction at >200 °C and mixing with colder, shallower groundwaters. The analysed waters were characterized by low abundance of dissolved solids (<150 p.p.m. Cl), with Si, Na, Cl and SO_4 being the dominant dissolved compounds.

Sinter growth studies were carried out in a wastewater drain ~15 m downstream of a steam separator (Fig. 8A). A slide tray was placed in a channel where the flow rate was 0.4 m s^{-1}, the average water temperature was 70 °C, and where the formation of sinters and biofilms was observed (Fig. 8A,B). The pH of the wastewater was slightly alkaline (pH 9.05 at 55 °C) and the total SiO_2 concentration was 304 p.p.m.

The XRD analyses of the fresh precipitates revealed calcite and small amounts of elemental sulphur as the main crystalline precipitates (Fig. 4; HV pattern); however, amorphous silica was clearly forming within and around the outflow channel. The precipitation of calcite within geothermal waters at Hveragerdi has been previously reported by Arnórsson (1978a). To verify the presence of amorphous silica, the crystalline calcite was removed by reacting with 10% HCl (weight loss of about 50%) and the remaining precipitate was re-analysed by XRD. This procedure exposed the characteristic broad peak of amorphous silica at 2θ of about 22.2° (Herdianita *et al.*, 2000). From the slides collected at Hveragerdi (Table 1, Fig. 8C), a silica precipitation rate of 0.7 ± 0.3 kg $year^{-1}$ m^{-2} was estimated.

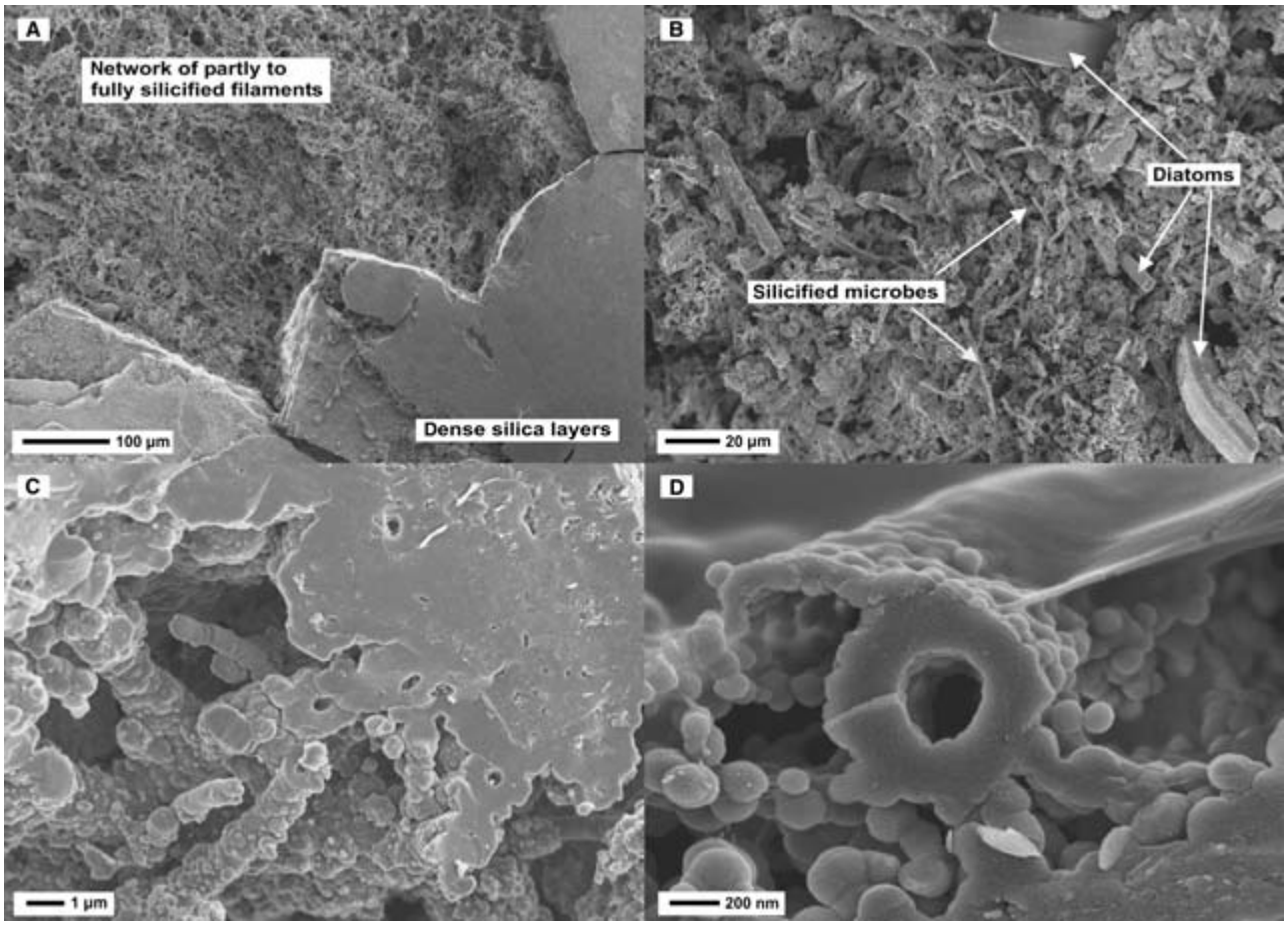

Fig. 7 Photomicrographs of slides collected at GY3 (after 3 months). (A) Compact network of microbial filaments (partly to fully silicified) in between dense blocks of amorphous silica. (B) Dense network of microbial filaments exhibiting different stages of silicification together with a few diatoms all associated with porous silica aggregates. (C) Silicified microbial filaments interdispersed between dense and thick layers of amorphous silica. (D) Close-up of an empty silica shell covered by silica nanoparticles that coalesced into a smooth silica layer.

As indicate in Fig. 8C, the AWI moved upwards over the 13 months course of the experiments which was probably the result of increased water flow from the steam separator (i.e. an increase in water depth within the outflow channel). Even though silica precipitates were present in the vicinity of the AWI, no dense and well-defined terraces or spicule-like structures developed. Both the top and the bottom of the slides were dominated by extensive biofilms (Fig. 9A) which were weakly to fully silicified and frequently interspersed with amorphous silica aggregates as well as calcite precipitates (Fig. 9A insert), with calcite precipitation primarily restricted to the submerged part of the slides.

Similar to the processes observed at GY3, on the slides from Hveragerdi, green-yellow and bright orange microbe-rich layers developed after about 8 months, suggesting the presence of photosynthesizing microorganisms (green-yellow) and orange pigmenting microbes (Fig. 8C). These biofilms formed above the AWI where temperatures were lower (~5 °C) than within the submerged parts of the slides, mimicking microbial mats that grew on sinters on the sides or within the wastewater drain (Fig. 8A,B). Slides collected after 3 and 5 months did not yet exhibit green or orange microbial layers, nevertheless, they were dominated by layers of silica and calcite densely populated with mats of filamentous microorganisms (Fig. 9a) as well as rod-shaped microbes and cocci (Fig. 9B). The degree of microbial silicification seemed to vary along the vertical length of the slides, with silicification being more pronounced in the upper parts close to the AWI. The comparison between the orange and the green layers (formed on the slides after 8 months) showed very similar textures that consisted primarily of a dense network of silicified filaments, empty silica shells and silica aggregates (Fig. 9C,D).

Reykjanes power station wastewater drain

The Reykjanes geothermal field is situated at the outermost tip of the Reykjanes peninsula (Fig. 1). The geothermal

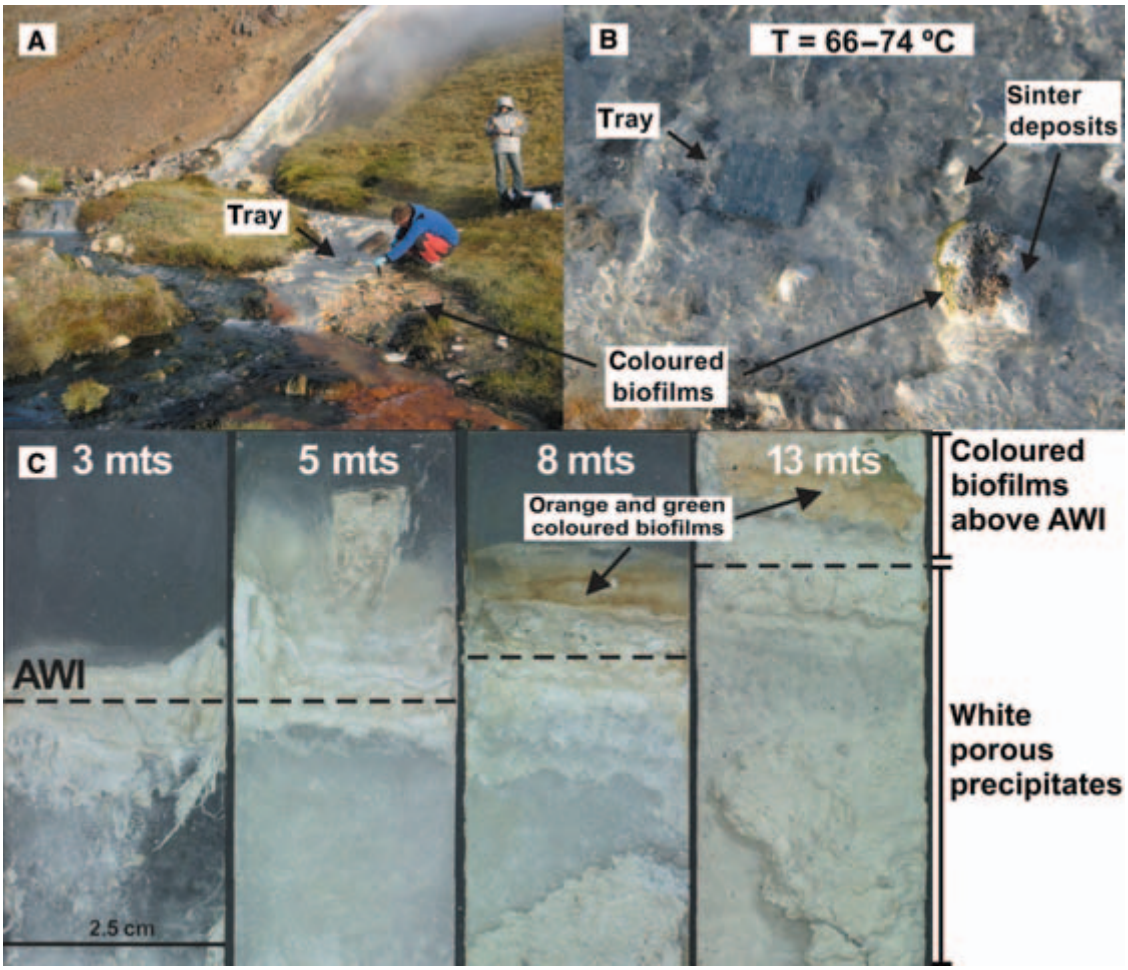

Fig. 8 (A) Outflow channel from the steam separator from Hveragerdi with marked position of the tray. (B) Close-up of sampling tray. (C) Slides collected from the tray over a time period of 13 months (mts). AWI, air–water interface.

waters are of seawater origin (Table 1) and have reacted with basalts at >250 °C (Arnórsson, 1978b). *In-situ* sinter growth experiments were carried out in a terraced, man-made wastewater drain of a steam separator (Fig. 10A). The flow rate at this site could not be determined with accuracy due to the terraced configuration of the outflow channel; however, a rate of 0.5–0.7 m s^{-1} was estimated. The temperature at the sampling site was 75 °C and the pH was near neutral (pH 7.50 at 39.8 °C). The measured total SiO_2 concentration within the studied wastewater was 695 p.p.m.

The base and sides of the wastewater drain were covered with thick deposits of white, soft, highly hydrated and porous precipitates (Fig. 10A). X-ray diffraction analysis (Fig. 4, RK pattern) showed that this porous material consisted of amorphous silica, with small amounts of halite and sylvite, the precipitation of which was solely due to drying of the untreated (unwashed) precipitates.

A first *in-situ* precipitation experiment was carried out for 5 days; however, after this time period, the whole tray was covered with soft and porous silica precipitate (Fig. 10B) and sampling of single slides (Fig. 10C) was not feasible without losing considerable amounts of material. Therefore, a second experiment with a much shorter time interval (Table 1, Fig. 10D) was carried out from which an average silica precipitation rate of 304 ± 20 kg $year^{-1}$ m^{-2} was estimated.

The second slide series showed that already after 30 min a fine layer of amorphous silica formed on the slides, and within 7.5 h the slides were covered with a 2-mm-thick porous layer (Fig. 10D). SEM analysis indicated homogeneous precipitates over the full vertical length of the slides consisting of aggregates of different sized silica spheres ranging from 11 nm up to 106 nm (mean diameter 43.2 ± 20.1 nm; $n = 140$; Fig. 11A). Interestingly, no microorganisms were observed within these porous precipitates. Elemental mapping using SEM-EDX analyses also failed to reveal traces of phosphate, or carbon, which could indicate the presence of microorganisms. However, this was not surprising as the high precipitation and flow rate also prevented the formation of microbial features (e.g. streamers, coloured mats) on the sides of the terraced wastewater drain. To further investigate whether this sampling

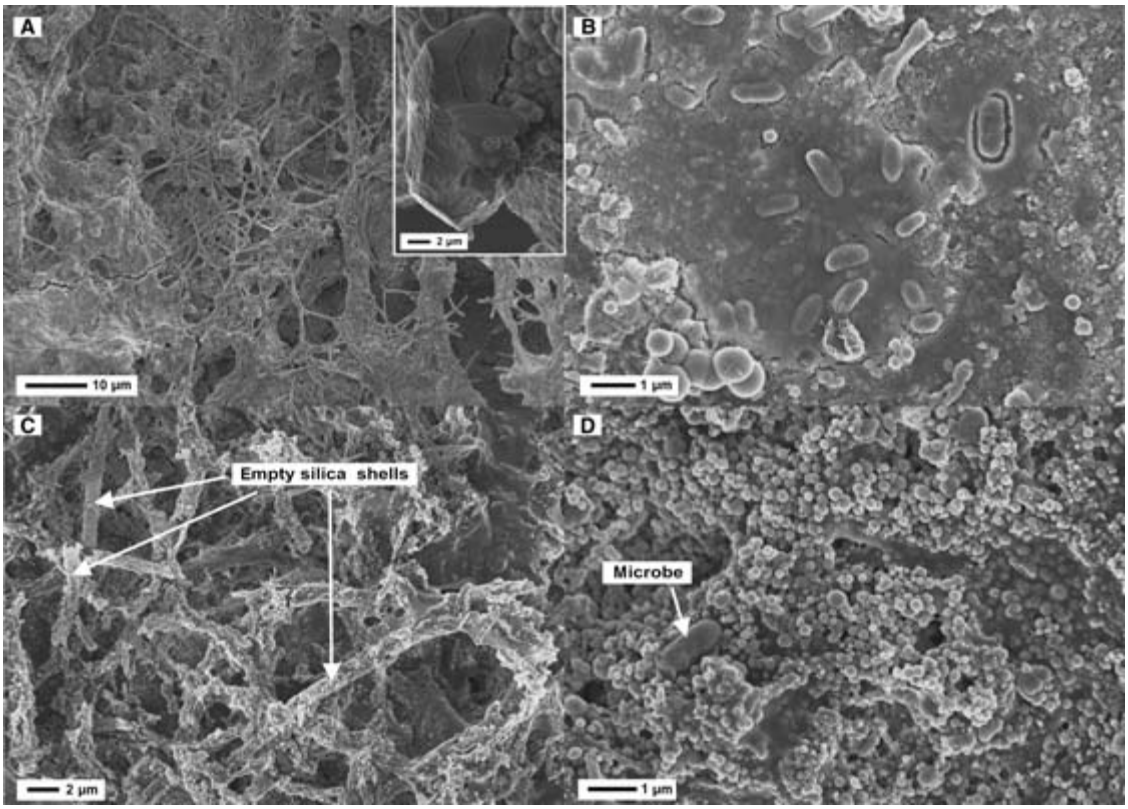

Fig. 9 Photomicrograph of slides collected at Hveragerdi (A–B: after 3 months, C–D: after 8 months). (A) Dense filamentous biofilm in the bottom parts of the slides; insert shows a calcite crystal. (B) Silica layers made up of small silica nanoparticles covering rod-or coccus-shaped microbes formed in the submerged parts of the slides. (C) Mix of silicified filaments, empty silica casings and silica aggregates. (D) Accumulation of silica nanospheres of different sizes forming layers interspersed with microbial cells (both C and D were close to the air–water interface.

location was poor or totally lacking in microbial activity, single-use, sterile filter papers used for water filtration were examined under the SEM, but again no microbial cells were found. It is worth mentioning that about 30 m further down the drain, a large standing pool (20 × 50 m, 40 °C) of wastewater had formed where the pool edges exhibited some green to yellow tainted sinters.

Svartsengi Power Station wastewater pool

Svartsengi Power Station is located on the Reykjanes peninsula about 20 km east of the Reykjanes Power Station (Fig. 1). The wastewaters from the power station exhibit an intense blue coloration (Fig. 12A) which is caused by the presence of colloidal silica suspended within the wastewater. The geothermal waters represent seawater–meteoric water mixtures (Table 1), with Na, Ca, K, and Cl being the most important elements.

Two sets of *in-situ* experiments (5 days, 17 days) were carried out in a pool (situated a few hundred metres downstream from a steam separator, Fig. 12A,B) where the water was mostly stagnant (low flow and controlled by wind and wave action). During the first set of experiments, the temperature at the study site was 42 °C and the pH was 7.7 (at 42 °C) while during the second set the temperature had increased to 60 °C, with no change in pH. The measured total SiO_2 concentration in the pool water was only 250 p.p.m., which was mainly a consequence of the fact that the bulk of the total silica (~630 p.p.m. after it leaves the steam separator; Thordarson & Tómasson, 1989) had already precipitated in large settling tanks located close to the steam separator outflow. In addition, the SV waters contained high loads of suspended colloidal silica (blue colour of the sampling pool, Fig. 12A,B) which, due to removal of suspended colloids during water filtration, led to an underestimation of the total silica concentration within the studied wastewater. XRD analysis showed amorphous silica as the sole precipitation phase with halite being present as a result of drying (<1% of total precipitate; Fig. 4, SV pattern).

From the first sinter growth experiment (Table 1), an average silica precipitation rate of 9.7 ± 3.5 kg $year^{-1}$ m^{-2} was determined, whereas from the second experiment, a slightly lower precipitation rate of 8.8 ± 3.4 kg $year^{-1}$ m^{-2} was obtained. It is important to note that the water temperature at the sampling

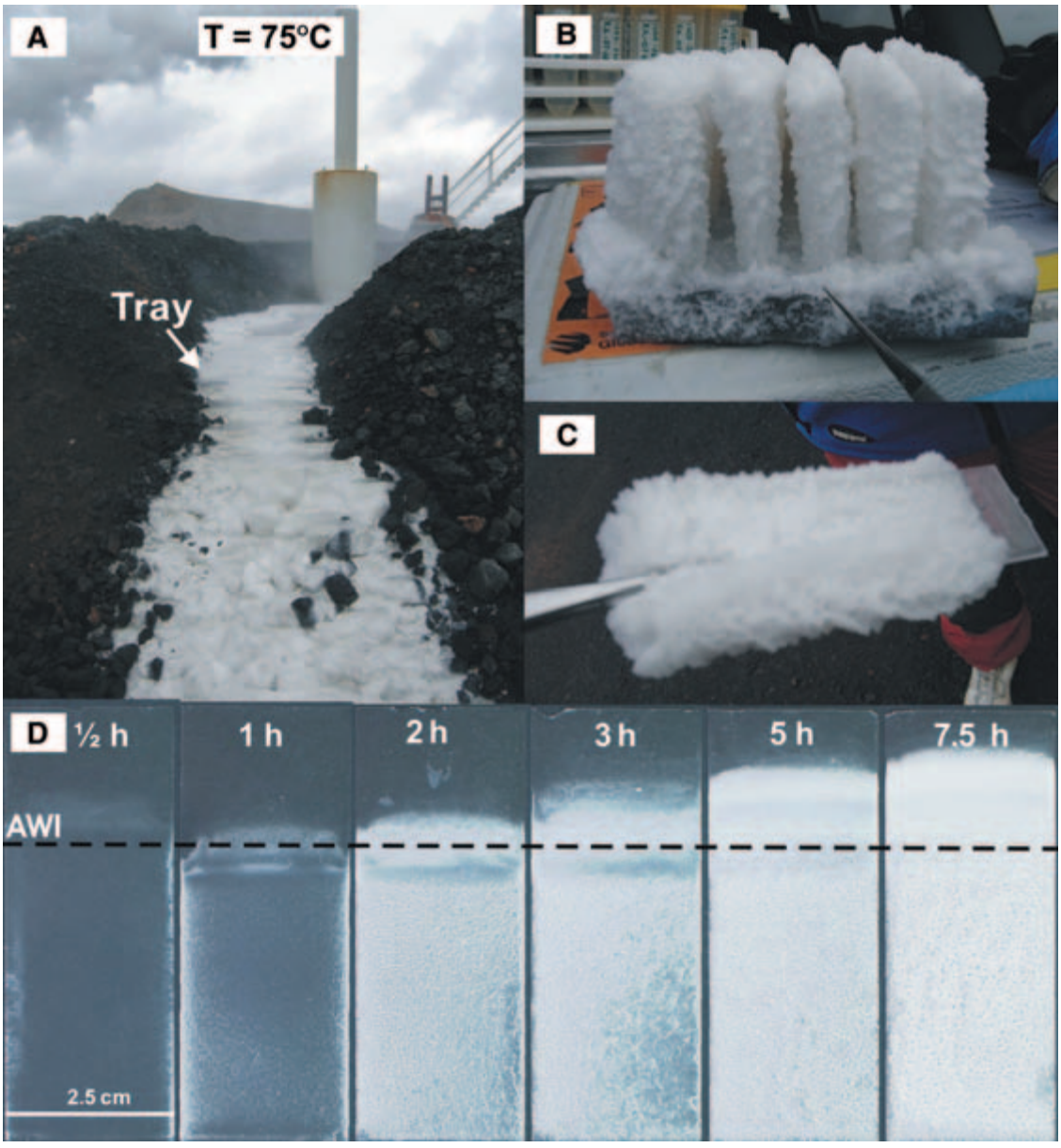

Fig. 10 (A) Outflow channel from a steam separator at Reykjanes Power Station. (B) Tray after 5 days. (C) Close-up of a single slide fully covered in soft and highly hydrated amorphous silica precipitates. (D) Glass slides collected from the second (short-term) experimental set as a function of time (h: hours). AWI, air–water interface.

site had increased from 42 to 60 °C between the two experimental sets, while all other parameters remained the same.

Microscopic analyses (SEM/EDX) of the precipitates on the slides revealed that over the full vertical length the slides were covered with fine aggregates of silica particles (Fig. 11B). Compared to Reykjanes, the SV aggregates were far smaller, more fragile and had an almost gel-like appearance where individual particles exhibited diameters between 10 and 36 nm (mean 18.4 ± 4.0 nm, n = 140, Fig. 11B). Similar to Reykjanes, the Svartsengi slides, as well as the filter paper used to collect the spring waters, revealed no traces of microorganisms.

Krafla Power Station wastewater drain

The Krafla geothermal area is situated in north eastern Iceland near Lake Mývatn and the volcano Krafla (Fig. 1). The fluids circulating within the geothermal system are dominated by meteoric water with increased concentrations of sulphate (Table 1), a consequence of interactions with basalts at >250 °C (Arnórsson *et al.*, 1983a).

The sampling location was situated in a wastewater drain of the Krafla Power Station where the temperature was 80 °C. The pH was very alkaline (pH 10.0) and the total SiO_2

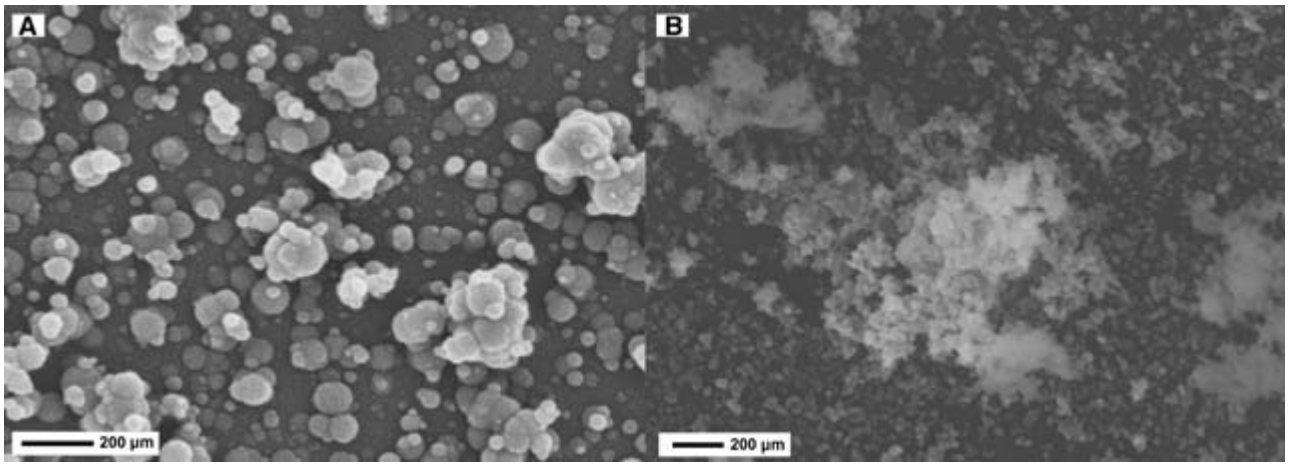

Fig. 11 (A) SEM photomicrographs of silica nanoparticles accumulated on slides collected at (A) Reykjanes after 1 h and (B) Svartsengi after 6 h.

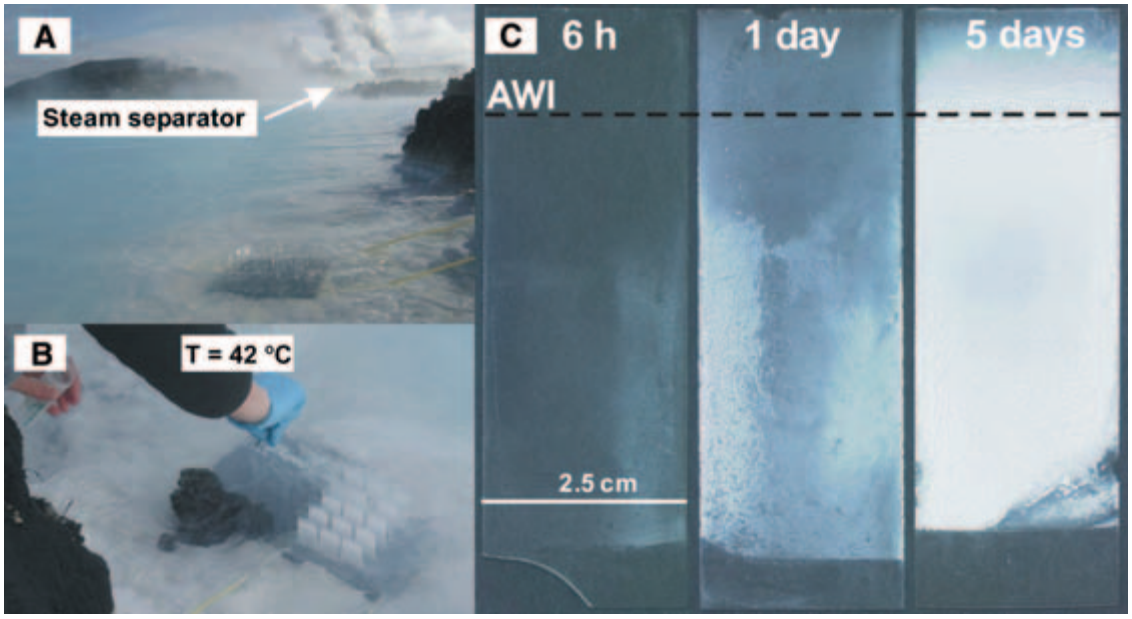

Fig. 12 (A) Blue wastewater pool at Svartsengi Power Station with sampling tray in the foreground. (B) Close-up of trays left for 6 h (left tray) and 5 days (right tray); note detail of sampling method. (C) Slides collected from the tray over a time period of 5 days. AWI, air–water interface.

concentration was 603 p.p.m. Hard and compact, black-coloured sinter deposits observed along the wastewater channel indicated relatively low sinter growth rates and therefore the tray and glass slides were sampled only once after 25 months. Surprisingly, the growth rate was far higher than expected and the whole tray was covered in dense, black precipitates (Fig. 13B,C). All slides were carefully separated and a precipitation rate of 19.5 ± 2.4 kg year^{-1} m^{-2} was estimated. XRD examination of fresh precipitates scraped off the top (Fig. 14, KF-T pattern) and bottom (Fig. 14, KF-B pattern) of the slides revealed that amorphous silica was the main mineral phase present within the black precipitate. Interestingly, the XRD pattern of the precipitates from the constantly submerged parts of the slides also revealed the presence of minor amounts of quartz (Fig. 14, KF-B, note small q-labelled peak above amorphous background). This could have either formed authigenically within the sinter (see discussion) or could be detrital and be brought to the surface by the circulating geothermal waters. However, it is noteworthy that no quartz crystals were identified by SEM.

The black colour of the precipitate was mainly caused by accessory minerals, including pyrrhotite, magnetite, and marcasite (Fig. 14, KF-T and KF-B pattern) which have all previously been identified as being in equilibrium with the geothermal waters at Krafla (Gunnlaugsson & Arnórsson, 1982). In addition, red precipitates were observed close to the AWI of the

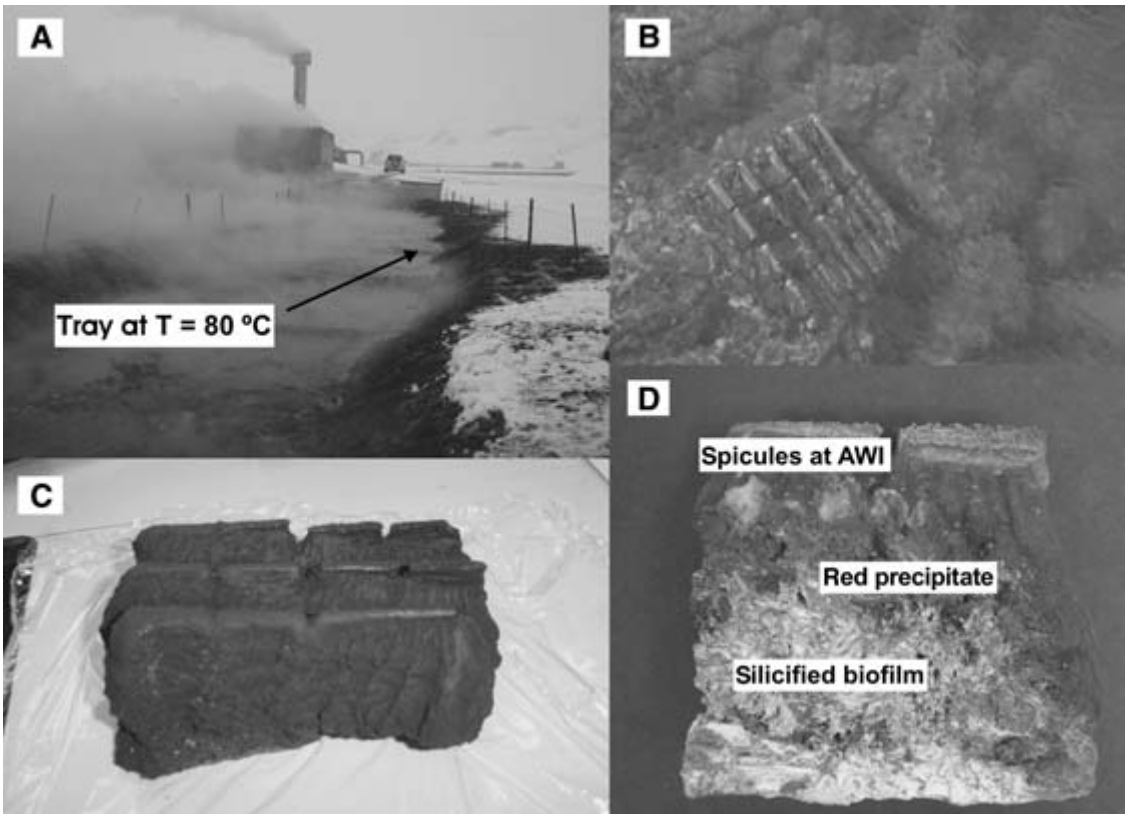

Fig. 13 (A) Steam separator and outflow channel at Krafla Power Station with location of sampling tray. (B) Close-up of tray left for 25 months within the wastewater drain. (C) Coalesced slides on the tray after collection. (D) Close-up of two separated and dried slides showing a heterogeneous texture and colour.

slides (Fig. 13D) consisting primarily of hematite (red colour), magnetite, marcasite and albite (Fig. 14, KF-R pattern). Pyrrhotite was absent within this red layer, indicating a possible oxidation of the sulfides to their oxide counterparts, i.e. hematite. Note that the precipitation of albite, iron sulphides and oxides contributed only little (<5%) to the measured growth rate as indicated by XRD (XRD peaks of these crystalline minerals are small compared to the broad opal-A peak).

All glass slides were covered with a 0.5- to 1-cm-thick layer of compact black sinter (Fig. 13) which made a microscopic examination of individual slides difficult, and thus precipitates, scraped off close to the AWI, the middle (including the red precipitates) and the bottom (thick biofilms) of the slides, were analysed. At the AWI, columnar textures developed consisting mainly of spherical aggregates of amorphous silica with few interspersed larger iron sulphides and oxides (confirmed by EDX and XRD; Fig. 14) and a few rod-shaped microorganisms (Fig. 15A). Further down the slide, the amount of microorganisms increased but overall, the slides were dominated by perfectly smooth silica spheres (that coalesced into larger aggregates; Fig. 15B) and a few larger crystals of iron oxides, sulfides and albite (Figs 15C and 14). In the constantly submerged parts of the slides, thick silicified biofilms dominated (Fig. 13D), consisting of long and fully silicified filaments (Fig. 15D) with lengths up to several hundreds of micrometres.

DISCUSSION

The main objectives of this study were threefold: (i) to quantify the growth rate of silica sinters as a function of temperature (42–96 °C), pH (7.5–10) and geothermal water composition (specifically silica content; 250–695 p.p.m.), (ii) to ascertain the variations in sinter structure and texture as a function of sinter growth rate and the presence/absence of microorganisms, and (iii) to compare and contrast these features.

As mentioned previously, a few studies (Mountain *et al.*, 2003; Smith *et al.*, 2003; Jones *et al.*, 2004 and Handley *et al.*, 2005) have carried out similar *in-situ* sinter growth studies in various geothermal areas in the Taupo volcanic zone in New Zealand, thus allowing a direct comparison between geothermal systems in Iceland and New Zealand. Similarly, *in-situ* growth studies (e.g. Blank *et al.*, 2002; Spear *et al.*, 2005; Kandianis *et al.*, 2008 and references therein) have been done in Yellowstone National Park, USA, however, no actual sinter growth rates were determined or they concentrated on calcite precipitation, i.e. formation of travertine, thus a comparison with these studies was not possible.

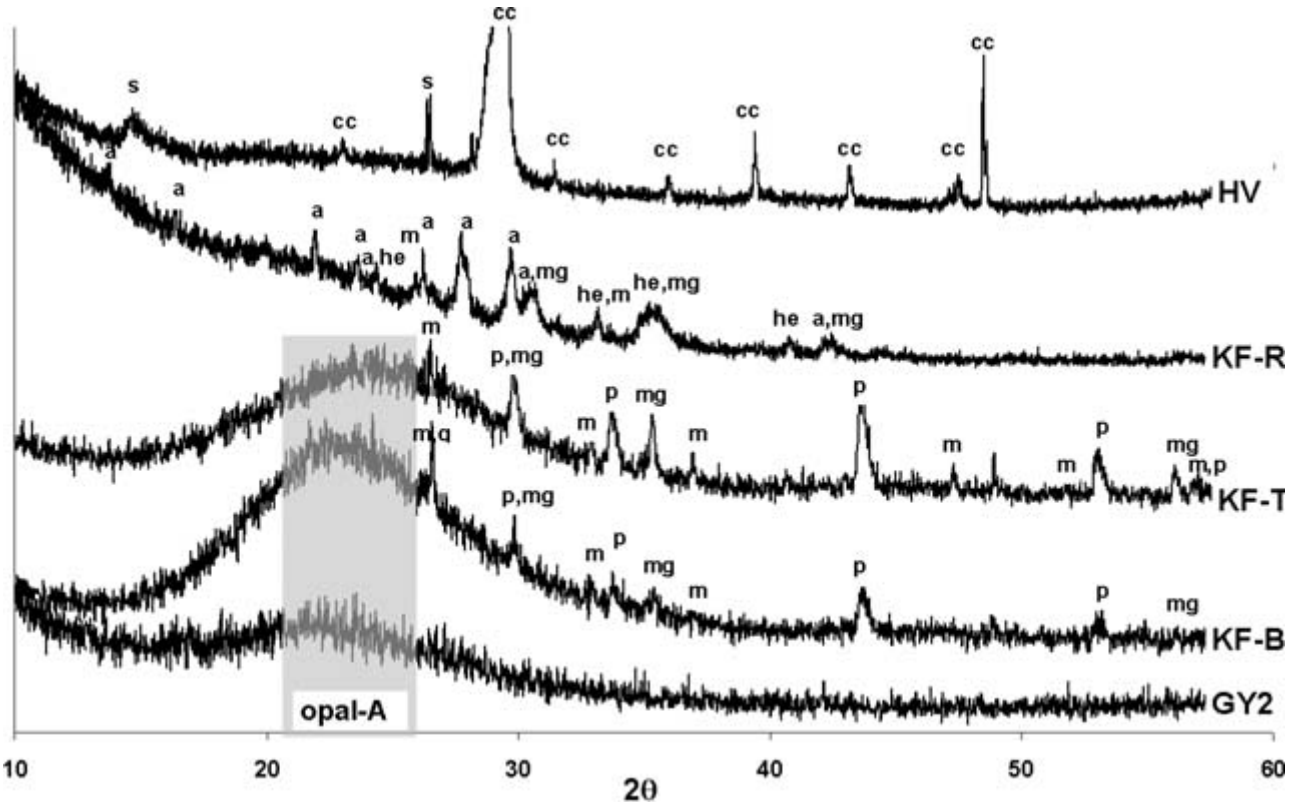

Fig. 14 X-ray powder diffraction (XRD) patterns of precipitates scraped off different parts of the slides collected at Krafla (top of slide, KF-T; bottom of slide, KF-B; red precipitate, KF-R). For comparison, the XRD patterns from Hveragerdi (HV) and Geysir (GY2) and the position of the opal-A 2θ-range are shown. a: albite, cc: calcite, he: hematite, m: marcasite, mg: magnetite, p: pyrrhotite, q: quartz, s: sulfur.

Table 2 Comparison of physico-chemical parameters of the studied geothermal waters as well as measured silica precipitation (ppt) rate and degree of silica saturation (using PHREEQC)

Location	T (°C)*	pH/°C†	$[SiO_2]_{tot}$ p.p.m.	Salintiy‡ %	Silica ppt rate kg y^{-1} m^{-2}	Saturation index, SI
Krafla	80	10.0/50	603	0.06	19.5 ± 2.4	– 0.94
GY1	70–96	9.0/86	363	0.05	0.2 ± 0.1	– 0.54
GY2	76–82	8.7/78	372	0.05	0.7 ± 0.3	– 0.38
GY3§	61–70	9.0/68	372§	0.05§	1.4 ± 0.4	– 0.40
Hveragerdi	66–74	9.1/71	304	0.04	0.7 ± 0.3¶	– 0.49
Svartsengi	42	7.7/42	250	2.56	9.7 ± 3.5	– 0.09
60	7.6/21	–**	–**	8.8 ± 3.4	–**	
Reykjanes	75	7.5/40	695	4.67	304 ± 20	0.17

*Temperature fluctuations over the experimental period.

†Mean value of measured pH over time period studied (variations ± 0.2 units).

‡Calculated with the ion concentrations listed in Table 1.

§Water chemistry at GY3 was assumed to be identical to GY2 due to their proximity (~10 m).

¶Overall growth rate, including calcite and silica precipitation in equal amounts, was 1.4 ± 0.6 kg $year^{-1}$ m^{-2}.

**Solution composition during the second experimental period was assumed to be equal to that in the first experimental period.

Spring and drain water chemistry, pH and T-regimes

Within the geothermal areas at Geysir, Hveragerdi and Krafla, the spring and drain waters were characterized by low salinity and alkaline pH, whereas the geothermal waters at Svartsengi and Reykjanes were highly saline (seawater–meteoric water mixtures) with near neutral pH (Table 2). Temperature, one of the major controls on silica solubility, and one of the prime reasons for choosing the various experimental sites, ranged between 42 and 96 °C. Similarly, the measured total silica concentrations varied substantially between the five studied geothermal systems (695 p.p.m. to 250 p.p.m. SiO_2) with the highest values at Reykjanes and Krafla and the lowest at Svartsengi (Table 2). Note that specifically at Svartsengi

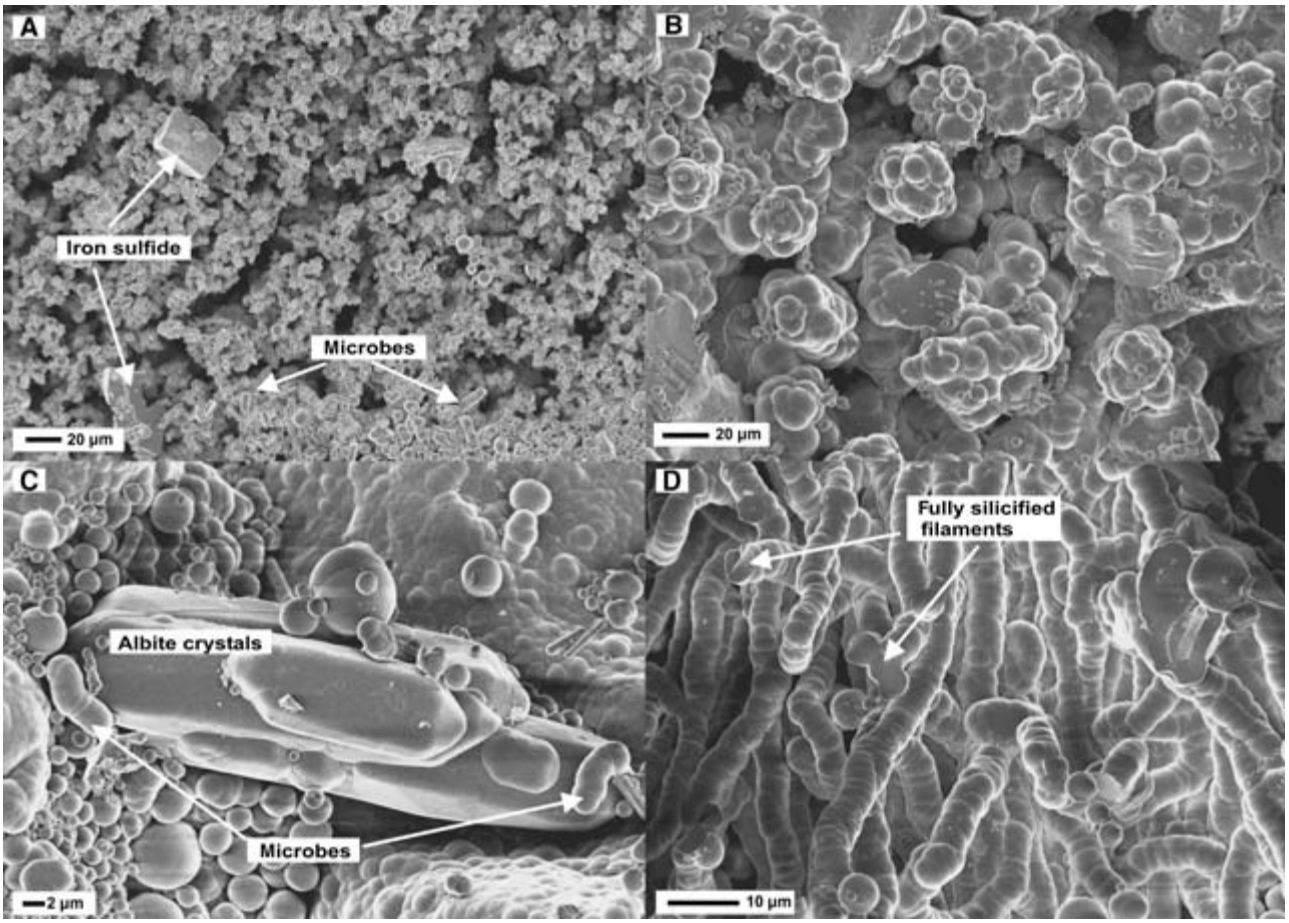

Fig. 15 Photomicrographs of precipitate from KF after 25 months. (A) Rough surface with columnar-like structures at the air–water interface consisting mainly of amorphous silica, iron sulphides and oxides (confirmed by EDX and XRD) interspersed with microbes and larger crystals of iron sulphides. (B) Aggregates of silica spheres. (C) Albite crystals surrounded by silica aggregates and microbes. (D) Dense accumulation of silicified microbial filaments in the lower parts of the slides.

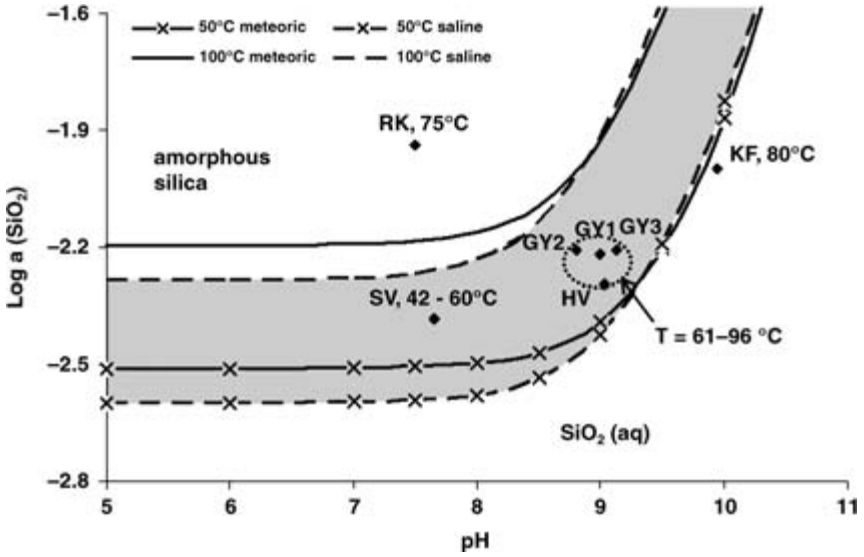

Fig. 16 Diagram of log activity (log (A) of silica as a function of pH, showing the effects of temperature and salinity. Also plotted are the pH – SiO_2 – conditions representing the five studied geothermal systems. The full lines depict the solubility of amorphous silica in meteoric waters at 50 and 100 °C whereas the shaded area represents the 50–100 °C silica solubility region in highly saline waters (contain ~ 0.7 M NaCl, represents salinity of geothermal waters at Reykjanes).

(and possibly at Reykjanes), filtration of the colloid-rich waters led to an underestimation of the measured total silica concentration in these waters.

The main factor governing silica precipitation from geothermal waters is silica solubility, i.e. degree of silica saturation, which is a function of pH, temperature, salinity and silica concentration (Fig. 16; e.g. Alexander, 1954; Goto, 1956; Iler, 1979; Makrides *et al.*, 1980; Marshall & Warakomski, 1980; Marshall & Chen, 1982). It follows that the degree of silica saturation (i.e. the rate of silica precipitation) is thus highest in near-neutral, saline, low-temperature geothermal waters with high silica concentrations (Fig. 16). As indicated by geochemical modelling with PHREEQC (see methods), the surface waters sampled at Geysir, Hveragerdi and Krafla appeared to be undersaturated with respect to amorphous silica (Table 2, $SI_{SiO2} < 0$ and Fig. 16), while the saline waters at Reykjanes were supersaturated (Table 2, $SI_{SiO2} > 0$ and Fig. 16; RK is significantly above the solubility lines). Despite its low temperature and near-neutral pH, the geothermal water at Svartsengi seemed slightly undersaturated with respect to amorphous silica (Table 2, $SI_{SiO2} \sim 0$). As mentioned above, this was due to the fact that the total silica concentration, i.e. SI value, was most likely underestimated due to removal of suspended silica colloids by filtration.

It should be noted that the calculated SI values are representative for equilibrated systems and this assumption is only partly valid for the studied waters. Furthermore, SI values can be substantially different if calculated with another geochemical code and a different database (data not shown). Therefore, the reported SI values most likely deviate from the true saturation state of the studied waters, but nevertheless provide information of the general trends.

Sinter growth rates

The variations in temperature, pH, salinity, silica concentration and abundance of microorganisms between the five studied Icelandic geothermal systems are reflected in the wide range of measured sinter growth rates (0.2 to 304 kg $year^{-1}\ m^{-2}$).

The effect of temperature is best exemplified by the growth rates determined at Svartsengi and the three Geysir sites. At Svartsengi, the differences in sinter growth rate between September 2005 (~10 kg $year^{-1}\ m^{-2}$ at 42 °C) and July 2007 (~9 kg $year^{-1}\ m^{-2}$ at 60 °C) were most likely the result of an increase in water temperature at the sampling sites. Similarly, the differences in growth rates between the three sampling sites at Geysir were best explained by the temperature-dependent solubility of amorphous silica (Iler, 1979) because at all Geysir sites pH, silica concentration and salinity were equivalent. As a result, the highest precipitation rates were measured at GY3 (1.4 kg $year^{-1}\ m^{-2}$, T_{max} = 70 °C) and the lowest at GY1 (0.2 kg $year^{-1}\ m^{-2}$) where the maximum temperature was about 26 °C higher (Table 2). The water temperature at GY2 (T_{max} = 82 °C) led to a growth rate (0.7 kg $year^{-1}\ m^{-2}$) in between the values determined for GY1 and GY3. These findings are consistent with the degree of silica saturation at GY1 (SI = –0.54) as compared to GY3 (SI = –0.40). It has to be noted that all studied spring waters at Geysir appeared to be undersaturated with respect to silica (Fig. 16, Table 2), suggesting that subaqueous silica precipitation was less favoured. This was in agreement with SEM results showing that sinters (spicular and layered structures) mostly formed close to the AWI due to evaporation and condensation processes. Similar observations were made by Mountain *et al.* (2003) in geothermal pools at Ngatamariki and Orakei Korako, New Zealand, in which sinter growth was also dominated by the formation of subaerial spicular structures. Note that the hydrodynamic and geochemical conditions at these sites were comparable with those in the Icelandic Geysir springs.

The geothermal waters at Hveragerdi had similar salinity, silica concentration, pH and temperature to GY3. After correction due to calcite precipitation, a silica precipitation rate of 0.7 kg $year^{-1}\ m^{-2}$ was calculated which is substantially lower compared to GY3 (1.4 kg $year^{-1}\ m^{-2}$). This lower rate is reflected in the lower SI at Hveragerdi (SI = –0.49) when compared with GY3 (SI = – 0.40, Fig. 16) and was due to the lower silica concentration in the waters at HV ($\Delta SiO_{2,\ GY3\text{-}HV}$ ~70 p.p.m.). As mentioned before, calcite precipitation was restricted to the submerged part of the slides while silica mainly formed in the vicinity of the AWI (Fig. 9). Equivalent processes have been described in geothermal waters in NZ, e.g. Orakei Korako (Mountain *et al.*, 2003) and Waikite (Jones *et al.*, 2000; Mountain *et al.*, 2003). At Waikite, only calcite was found to precipitate subaqueously at high temperatures, while at Orakei Korako, ~26% of the sinter growth contribution stemmed from subaqueous calcite precipitation with the remainder of the sinter growth being due to silica precipitation.

Much higher precipitation rates were observed for the saline waters at Reykjanes and Svartsengi. At Reykjanes, the waters were supersaturated with respect to amorphous silica (SI = 0.18, Fig. 16) and the measured growth rate (304 kg $year^{-1}\ m^{-2}$) was between 200- and 1000-fold higher than at Geysir and Hveragerdi. This high rate was the result of the high total silica concentration, the near neutral pH, and to a lesser extent, the high salinity of the drain waters. The Reykjanes growth rate is comparable to sinter growth rates within a wastewater drain at Wairakei Power Station, New Zealand (Mountain *et al.*, 2003), where a similar growth rate (350 kg $year^{-1}\ m^{-2}$) was measured, although the drain waters at Wairakei were colder (62 °C), more alkaline (pH = 8.5) and less saline (meteoric water origin), thus more comparable to Geysir and Hveragerdi. The similarity in growth rates between Wairakei and Reykjanes may be primarily the consequence of the fast re-supply of highly silica saturated solutions, while salinity and temperature may play a lesser role.

At Svartsengi, the growth rates (~9 kg year^{-1} m^{-2} at 60 °C and ~10 kg year^{-1} m^{-2} at 42 °C) were a thirtieth of those at Reykjanes. Although, salinity at both sites was high, the lower total silica concentration (measured after filtration and colloid removal), i.e. degree of silica saturation (SI = –0.09), and the slow re-supply of fresh silica-rich solution resulted in a much lower precipitation rate compared to Reykjanes. As mentioned previously, the bulk of the total silica had already precipitated in form of colloids along the outflow channels (blue colour in Fig. 12A). As a result, sinter growth at this site was mainly controlled by aggregation of the suspended silica colloids, and to a lesser extent by evaporation and cooling processes.

As illustrated in Fig. 16, the pH of geothermal waters has a strong effect on the solubility of amorphous silica and thus on sinter growth rates. Therefore, it was not surprising to find the most undersaturated waters at Krafla (SI = –0.94) where the geothermal water had a pH of 10 (silica solubility at pH 10 is more than twice as high as at pH 9, Fig. 16). However, the precipitation rate determined for Krafla (19.5 kg year^{-1} m^{-2}) was ~10 times higher than within the geothermal waters at Geysir and Hveragerdi although the waters at all these three sites were of equivalent salinity and temperature. Furthermore, the Krafla rate was twice as high as at Svartsengi where the wastewaters were highly saline, near neutral, lower in temperature and contained high amounts of suspended silica particles. As shown by the SEM analyses of the Krafla precipitates (Fig. 15A,B), substantial amounts of silica precipitated in the vicinity of the AWI due to evaporation and condensation processes. However, most silica was found in the submerged parts of the slides which were covered by thick silicified biofilms (Figs 13D and 15D). This suggests that once the slides were densely colonized by microorganisms, silica particles that formed close to the AWI (due to cooling and evaporation processes) quickly adhered to the surfaces of the biofilm leading to its complete silicification (e.g. Mountain *et al.*, 2003; Benning *et al.*, 2004a,b). Particle adhesion/aggregation most likely occurred via hydrogen bonding and entrapment of particles within the complex structures of the biofilms exopolysaccharides (e.g. Benning *et al.*, 2004a; Tobler, 2008). Also note that at Krafla the total silica concentration was twice as high as at Geysir and Hveragerdi, which resulted in a substantially higher polymerization and precipitation rate in the vicinity of the AWI.

Comparison of sinter growth rates and structures/textures

Overall, in the five studied geothermal areas, the influence of microorganisms on the texture and structure of sinters was variable but, the sinter fabrics correlated well with the growth rates determined at each locality as well as other *in-situ* studies (e.g. Mountain *et al.*, 2003; Handley *et al.*, 2005).

In spring and drain waters at Geysir and Hveragerdi where the precipitation rates were low, sinter fabrics consisted of dense, weakly laminated and quite heterogeneous deposits. The sinter structures and textures were dominated by the high abundance of thermophilic microorganisms (60 to 96 °C), and biofilms mainly developed subaqueously. For example, at GY1 and GY2, after only 5 days filamentous microorganisms fully covered the submerged parts of the slides where the temperatures were consistently ~80 °C. Even at the AWI where the water temperature reached values as high as 96 °C (i.e. GY1) microorganisms were still present. Note that subaqueous silica precipitation was restricted at these sites (i.e. undersaturated waters), yet, these biofilms slowly became silicified by providing surfaces for the adhesion and aggregation of silica particles (see above). This silicification process did not happen rapidly (i.e. low precipitation rates) but rather took weeks to months, leading to the full silicification of the microbial communities and the subsequent incorporation into the compact sinters (Handley *et al.*, 2005). Nevertheless, at GY1 and GY2 after only 5 days, microorganisms were already partly silicified. Similar high silicification rates were observed in a spring outflow channel at Krisuvik, Iceland (Konhauser *et al.*, 2001), as well as in geothermal waters in New Zealand, e.g. Iodine Pool, Waimangu (Jones *et al.*, 2004) and Champagne Pool, Waiotapo (e.g. Jones *et al.*, 1999; Handley *et al.*, 2005).

The textures that dominated the vicinity of the AWI at GY1 and GY2 included compact silica layers interspersed with spicules and terrace-like structures, which were sporadically covered with microorganisms. The best defined spicules were observed at GY1 which were analogous to those observed at Octopus Spring, Yellowstone National Park (a gently surging, near-neutral spring with T varying from <73 to >85 °C, Braunstein & Lowe, 2001). A few spicules also formed on slides collected at GY2; however, the dominant features at the AWI were distinct silica terraces that increased in height up to 3 mm over the time period studied (Fig. 3D). These terraces resembled the subaerially formed sinter bands on slides collected from Champagne Pool, New Zealand (pH = 5.5 and T = 75 °C, meteoric water origin; Handley *et al.*, 2005).

At sites with lower temperatures, i.e. GY3 and HV, microbial mats colonized the slides faster, and the range of microbial cell morphologies was significantly higher than at GY1 and GY2 (higher temperatures). This larger diversity was confirmed by 16S rDNA analysis of microbial mats from these sites (Tobler, 2008). On slides from GY3 and HV, coloured biofilms also developed at the AWI (Figs 8 and 11) which inhibited the development of spicules and well-defined terraces. The features observed at these two sites can be compared with those at Pavlova spring, Ngatamariki, New Zealand (pH = 7.2, T = 71 °C, Mountain *et al.*, 2003) where biofilms fully covered the slides after only 6 days.

At Krafla, the textures and structures of the black sinters were comparable to GY1 and GY2 where most silica precipitated in the vicinity of the AWI (subaerially) and the bottom parts of the slides were dominated by fully silicified and well-preserved biofilms. However, compared to all other sites, a substantially higher variety of minerals were detected in the Krafla precipitates,

e.g. quartz, albite and various iron sulfides and oxides. In these settings, quartz was most probably of detrital origin and was brought to the surface by the circulating geothermal waters interacting with the basaltic host rocks. However, Lynne *et al.* (2006) showed that quartz may also form authigenically via the ageing of amorphous silica immersed for ~5–24 months in a low pH (3.5–5.5), high temperature (75–94 °C) steam vent at Orakei Korako, New Zealand. Such an ageing/transformation of amorphous silica to quartz is less feasible in the Krafla sinters (25 months exposure, 80 °C) due to the much higher pH (pH = 10) of the reacting solutions and thus a detrital origin is more plausible. Similarly to quartz, albite is not a common mineral in 'fresh' sinter deposits but it has been shown to occur as an alteration product in both low and high temperatures geothermal environments (e.g. Miyashiro, 1975; Browne, 1978; and references therein). Furthermore, Stefánsson & Arnórsson (2000) demonstrated that geothermal waters are in equilibrium with low albite at temperatures between 20 to 300 °C.

Lastly, at Svartsengi and Reykjanes where the precipitation rates were intermediate to very high, sinters forming within and along the wastewater drains and pools (both subaqueous and subaerially) were very porous and homogeneous. It is worth noting that particle interactions are aided by the presence of salts (i.e. interparticle bonding through cations such as Na^+; e.g. Iler, 1979; Smith *et al.*, 2003). This suggests that silica particle aggregation was enhanced in the highly saline geothermal waters at Svartsengi and Reykjanes which also explained the formation of the porous, gel-like precipitates in these waters. Intriguingly, the size distribution of the silica aggregates as well as of the individual silica nanoparticles differed between the two sampling locations. At Reykjanes, at higher temperature and precipitation rate, a wider size distribution was observed (11–106 nm), while at Svartsengi (far lower temperatures, slower precipitation rates and stagnant water) a very narrow distribution of the individual silica particles (10–36 nm) was observed. From these data, it is not possible to pinpoint the governing factor leading to this discrepancy and most probably more than one factor, e.g. temperature, precipitation rate as well as flow rate, influences the size of the precipitating silica colloids (Tobler, 2008).

The high precipitation rates as well as high salt contents at Reykjanes and Svartsengi were also not conducive to microbial colonization and SEM observation of slides or filters from both sites failed to reveal any microbial presence. However, successful DNA extraction from sediments collected at Svartsengi (next to the tray; Tobler, 2008) indicated that over longer periods, microorganisms adapted to the conditions present in the studied pool. In contrast, DNA extraction at Reykjanes was not successful (Tobler, 2008) which suggested that due to the high salinity, high temperature, high flow rate as well as high sinter growth rate (304 kg $year^{-1}$ m^{-2}) the microbial abundance was low at this site.

CONCLUSIONS

In-situ sinter growth experiments carried out in geothermal areas are uniquely suited to provide data on the mechanisms and processes affecting or governing sinter formation as a function of a complex set of parameters. In this study, growth rates and the structural and textural developments of sinters from five diverse geothermal sites in Iceland were analysed from both an abiotic and a biotic perspective. The fact that the physico-chemical conditions varied significantly between these sites allowed a realistic comparison of sinter growth rates, sinter structures and textures between the different hydrodynamic and geochemical settings. The results clearly showed that the mesoscopic and microscopic textural development of silica sinters was strongly influenced by (i) the inorganic silica precipitation rate which itself was a function of temperature, pH, salinity, silica concentration and flow rates; (ii) the precipitation mechanism (subaqueously and/or subaerially) and (iii) the presence of mesophilic and thermophilic microorganisms. In all geothermal areas where the waters exhibited near neutral pH, high silica content and moderate to high salinity (i.e. Svartsengi and Reykjanes, respectively), silica precipitation rates were high. These physico-chemical parameters led to the growth of porous and homogeneous sinters that developed predominantly subaqueously. In addition, due to the high salt contents and high growth rates, microbial abundance was very low and microbial fossilization and preservation was poor. Conversely, in the geothermal sites where the waters appeared to be undersaturated with respect to silica (i.e. Geysir, Hveragerdi and Krafla), subaqueous silica precipitation was restricted and sinter growth was mostly observed at the AWI where evaporation and condensation processes dominated. As a consequence, dense and heterogeneous sinters with well-defined spicules and silica terraces formed in the vicinity of the AWI. Despite the high temperatures of these geothermal waters, the submerged zones were quickly (<5 days) colonized with extensive biofilms, which in turn acted as surfaces for and possibly also enhanced the aggregation/adhesion of inorganically formed silica nanoparticles. Ultimately, this led to the build up of fairly complex and diverse silica sinter structures and textures with fully silicified and well-preserved biofilms.

These results substantiate the strong abiotic–biotic relationship and the important role of microorganisms in geothermal settings to act as surfaces for sinter formation. Naturally, the observed processes also emphasize the importance of *in-situ* studies in natural settings with a view towards enhancing our understanding of processes on the modern Earth, but with equivalent applications to ancient geological processes observed on the Precambrian Earth. Lastly, silica-rich deposits recently described in Gusev Crater on Mars were postulated possibly to have derived from hydrothermal solutions supersaturated in silica. Although, obviously so far no microbial evidence has been documented, the preponderance

and close association of microbial communities with silica sinters on Earth make this a good analogue for future missions to Mars.

ACKNOWLEDGEMENTS

Special thanks to Vernon Phoenix (Glasgow University, UK) and Hanna Sisko Kaasalainen (University of Iceland) for field sampling assistance and to Stefan Arnórsson (University of Iceland) for helping with field logistics. DJT would also like to thank Bruce Mountain (GNS Science, New Zealand) for ICP-OES analyses, Stefan Hunger for IC analyses and Juan Diego Rodrigues Blanco (University of Leeds, UK) for his help with geochemical modelling. This research was funded by a PhD fellowship from the Earth and Biosphere Institute (University of Leeds, UK), with field work support from the Geological Society of Great Britain and Ireland (Timothy Jefferson Field Research Fund), and the University of Leeds funding (LGB) as well as Icelandic Research Council grants (AS). We also thank the three anonymous reviewers and Kurt Konhauser for their valued comments.

REFERENCES

Alexander GB (1954) The polymerization of monosilicic acid. *Journal of the American Chemical Society* **76**, 2094–2096.

Arnórsson S (1975) Application of silica geothermometer in low-temperature hydrothermal areas in Iceland. *American Journal of Science* **275**, 763–784.

Arnórsson S (1978a) Precipitation of calcite from flashed geothermal waters in Iceland. *Contributions Mineralogical Petrology* **66**, 21–28.

Arnórsson S (1978b) Major element chemistry of geothermal seawater at Reykjanes and Svartsengi, Iceland. *Mineralogical Magazine* **42**, 209–220.

Arnórsson S (1985) The use of mixing models and chemical geothermometers for estimating underground temperatures in geothermal systems. *Journal of Volcanology and Geothermal Research* **23**, 299–335.

Arnórsson S, Gunnlaugsson E, Svavarsson H (1983a) The chemistry of geothermal waters in Iceland. II. Mineral equilibria and independent variables controlling water compositions. *Geochimica et Cosmochimica Acta* **47**, 547–566.

Arnórsson S, Gunnlaugsson E, Svavarsson H (1983b) The chemistry of geothermal waters in Iceland. III. Chemical geothermometry in geothermal investigations. *Geochimica et Cosmochimica Acta* **47**, 567–577.

Ball JW, Nordstrom DK (1992) Geochemical model to calculate speciation of major, trace and redox elements in waters. US Geological Survey, International Groundwater Modeling Centre, Golden, Colorado, 189 pp.

Benning LG, Phoenix VR, Yee N, Konhauser KO (2004a) The dynamics of cyanobacterial silicification: an infrared micro-spectroscopic investigation. *Geochimica et Cosmochimica Acta* **68**, 729–741.

Benning LG, Phoenix VR, Yee N, Tobin MJ (2004b) Molecular characterization of cyanobacterial silicification using synchrotron infrared micro-spectroscopy. *Geochimica et Cosmochimica Acta* **68**, 743–757.

Blank CE, Cady SL, Pace NR (2002) Microbial composition of near-boiling silica depositing thermal springs throughout Yellowstone National Park. *Applied Environmental Microbiology* **68**, 5123–5135.

Braunstein D, Lowe DR (2001) Relationship between spring and geyser activity and the deposition and morphology of high temperature (>73 °C) siliceous sinter, Yellowstone National Park, Wyoming, USA. *Journal of Sedimentary Research* **71**, 747–763.

Brock TD (1978) *Thermophilic Microorganisms and Life at High Temperatures*. Springer-Verlag, New York, pp. 465.

Browne PRL (1978) Hydrothermal alteration in active geothermal fields. *Annual Review of Earth and Planetary Sciences* **6**, 229–250.

Cady SL, Farmer JD (1996) Fossilization processes in siliceous thermal springs trends in preservation along thermal gradient. In *Evolution of Hydrothermal Ecosystem on Earth (and Mars?)*. Ciba Foundation, Wiley, New York, pp. 150–172.

Chung AP, Rainey FA, Valente M, Nobre MF, da Costa MS (2000) *Thermus igniterrae* sp. nov and *Thermus antranikianii* sp. nov., two new species from Iceland. *International Journal of Systematic and Evolutionary Microbiology* **50**, 209–217.

Ferris FG, Beveridge TJ, Fyfe WS (1986) Iron-silica crystallite nucleation by bacteria in a geothermal sediment. *Nature* **320**, 609–611.

Goto K (1956) Effect of pH on polymerization of silicic acid. *Journal of Physical Chemistry* **60**, 1007–1008.

Greenberg AE, Trussell RR, Clesceri L (1985) *Standard Methods for the Examination of Water and Wastewater*. American Public Health Association, New York, 209 pp.

Guidry SA, Chafetz HS (2003) Factors governing subaqueous siliceous sinter precipitation in hot springs: examples from Yellowstone National Park, USA. *Sedimentology* **49**, 1253–1267.

Gunnarsson I, Arnórsson S (2000) Amorphous silica solubility and the thermodynamic properties of H_4SiO_4 in the range of o to 350 °C at P_{sat}. *Geochimica et Cosmochimica Acta* **64**, 2295–2307.

Gunnarsson I, Arnórsson S (2003) Silica scaling: the main obstacles in efficient use of high-temperature geothermal fluids. International Geothermal Conference, Reykjavik, 30–36.

Gunnlaugsson E, Arnórsson S (1982) The chemistry of iron in geothermal systems in Iceland. *Journal of Volcanology and Geothermal Research* **14**, 281–299.

Handley KM, Campbell KA, Mountain BW, Browne PRL (2005) Abiotic–biotic controls on the origin and development of spicular sinter: *in situ* growth experiments, Champagne Pool, Waiotapu, New Zealand. *Geobiology* **3**, 93–114.

Herdianita NR, Browne PRI, Rodgers KA, Campbell KA (2000) Mineralogical and textural changes accompanying ageing of silica sinter. *Mineralium Deposita* **35**, 48–62.

Hinman NW, Lindstrom RF (1996) Seasonal changes in silica deposition in hot spring systems. *Chemical Geology* **132**, 237–246.

Hjorleifsdottir S, Skirnisdottir S, Hreggvidsson GO, Holst O, Kristjansson JK (2001) Species composition of cultivated and noncultivated bacteria from short filaments in an Icelandic hot spring at 88 °C. *Microbial Ecology* **42**, 117–125.

Iler RK (1979) *The Chemistry of Silica*. John Wiley, New York.

Jones B, Kronhauser KO, Renaut RW, Wheeler RS (2004) Microbial silicification in Iodine Pool, Waimangu geothermal area, North Island, New Zealand: implications for recognition and identification of ancient silicified microbes. *Journal of the Geological Society London* **161**, 983–993.

Jones B, Renaut RW, Rosen MR (1997) Biogenicity of silica precipitation around geysers and hot spring vents, North Island, New Zealand. *Journal of Sedimentary Research* **67**, 88–104.

Jones B, Renaut RW, Rosen MR (1998) Microbial biofacies in hot springs sinters: a model based on Ohaaki pool, North Island, New Zealand. *Journal of Sedimentary Research* **68**, 413–434.

Jones B, Renaut RW, Rosen MR (1999) Actively growing siliceous oncoids in the Waiotapu geothermal area, North Island, New Zealand. *Journal of the Geological Society, London* **156**, 89–103.

Jones B, Renaut RW, Rosen MR (2000) Trigonal dendritic calcite crystals forming from hot spring waters at Waikite, North Island, New Zealand. *Journal of Sedimentary Research* **70**, 586–603.

Kandianis MT, Fouke BW, Johnson RW, Veysey IIJ, Inskeep WP (2008) Microbial biomass: a catalyst for $CaCO_3$ precipitation in advection-dominated transport regimes. *Geological Society of America Bulletin* **120**, 442–450.

Konhauser KO, Ferris FG (1996) Diversity of iron and silica precipitation by microbial mats in hydrothermal waters, Iceland: implications for Precambrian iron formations. *Geology* **24**, 323–326.

Konhauser KO, Phoenix VR, Bottrell SH, Adams DG, Head IM (2001) Microbial–silica interactions in Icelandic hot springs sinter: possible analogues for some Precambrian siliceous stromatolites. *Sedimentology* **48**, 415–433.

Kristmannsdóttir H (1989) Types of scaling occuring by geothermal utilization in Iceland. *Geothermics* **18**, 183–190.

Kvist T, Ahring BK, Westermann P (2007) Archaeal diversity in Icelandic hot springs. *FEMS Microbiology Ecology* **59**, 71–80.

Lalonde SV, Konhauser KO, Reysenbach AL, Ferris FG (2005) The experimental silicification of Aquificales and their role in hot spring formation. *Geobiology* **3**, 41–52.

Lynne BY, Campell KA, Perry RS (2006) Alteration of sinter diagenesis in an active fumarole, Taupo volcanic zone, New Zealand. *Geology* **34**, 749–752.

Makrides AC, Turner M, Slaughter J (1980) Condensation of silica from supersaturated silicic acid solutions. *Journal of Colloid and Interface Science* **73**, 345–367.

Marshall WL, Chen CTA (1982) Amorphous silica solubilities – V. Predictions of solubility behaviour in aqueous mixed electrolyte solutions to 300 °C. *Geochimica et Cosmochimica Acta* **46**, 289–291.

Marshall WL, Warakomski JM (1980) Amorphous silica solubilities – II. Effect of aqueous salt solutions at 25 °C. *Geochimica et Cosmochimica Acta* **44**, 915–924.

McKenzie EJ, Brown KL, Cady SL, Campell KA (2001) Trace metal chemistry of microorganisms in geothermal sinter, Taupo Volcanic Zone, New Zealand. *Geothermics* **30**, 483–502.

Miyashiro A (1975) *Metamorphism and Metamorphic Belts.* Allen & Unwin, London, 492 pp.

Mountain BW, Benning LG, Boerema J (2003) Experimental studies on New Zealand hot spring sinters: rates of growth and textural development. *Canadian Journal of Earth Sciences* **40**, 1643–1667.

Parkhurst DL, Appelo CAJ (1999) User's guide to PHREEQC (version 2)-A computer program for speciation, batch-reaction, one-dimensional transport, and inverse geochemical calculations. US Geological Survey, Water-Resources Investigations Report 99-4259, 312 pp.

Pétursdóttir SK, Kristjánsson JK (1996) The relationship between physical and chemical conditions and low microbial diversity in the Blue Lagoon geothermal lake in Iceland. *FEMS Microbiology Ecology* **19**, 39–45.

Phoenix VR (2001) Microbial–biomineral interactions and their significance for the formation of chemical sediments. PhD thesis, University of Leeds, Leeds, UK.

Renault RW, Jones B, Rosen MR (1996) Primary silica oncoids from Orakeikorako hot springs, North Island, New Zealand. *Palaios* **11**, 446–458.

Ruff SW, Farmer JD, Calvin WM, Johnson JR, Arvidson RE, Squyres SW, Christensen PR, Team TS (2007) Evidence for a possible siliceous sinter deposit at Home Plate in Gusev Crater. *Eos Transactions, AGU* **88**, P23A-1097 (abstract).

Schinteie R, Campbell KA, Browne PRL (2007) Microfacies of stromatolitic sinter from acid-sulphate-chloride springs at Parariki Stream. Rotokawa geothermal field, New Zealand. *Palaeontologia Electronica* **10**, 33.

Schultze-Lam S, Ferris FG, Kronhauser KO, Wiese RG (1995) In situ silicification of an Icelandic hot spring microbial mat: implications for microfossil formation. *Canadian Journal of Earth Sciences* **32**, 2021–2026.

Skírnisdóttir S, Hreggvidsson GO, Hjörleifsdottir S, Marteinsson VT, Pétursdóttir SK, Holst O, Kristjánsson JK (2000) Influence of sulfide and temperature on species composition and community structure of hot spring microbial mats. *Applied and Environmental Microbiology* **66**, 2835–2841.

Smith BY, Turner SJ, Rodgers KA (2003) Opal-A and associated microbes from Wairakei, New Zealand: the first 300 days. *Mineralogical Magazine* **67**, 563–579.

Sonne-Hansen J, Ahring BK (1997) Anaerobic microbiology of an alkaline Icelandic hot spring. *FEMS Microbiology Ecology* **23**, 31–38.

Spear JR, Walker JJ, McCollom TM, Pace NR (2005) Hydrogen and bioenergetics in the Yellowstone geothermal ecosystem. *Proceedings of the National Academy of Sciences of the USA* **102**, 2555–2560.

Squyres SW, Arvidson RE, Ruff S, Gellert R, Morris RV, Ming DW, Crumpler L, Farmer JD, Des Marais DJ, Yen A, McLennan SM, Calvin W, Bell JF, IIIClark BC, Wang A, McCoy TJ, Schmidt ME, de Souza PA Jr (2008) Detection of silica-rich deposits on Mars. *Science* **320**, 1063–1067.

Stefánsson A, Arnórsson S (2000) Feldspar saturation state in natural waters. *Geochimica et Cosmochimica Acta* **64**, 2567–2584.

Thordarson H, Tómasson TH (1989) Brine classification at Svartsengi, Iceland: effect of pH and temperature on the precipitation of silica and its properties. *Geothermics* **18**, 287–294.

Tobler DJ (2008) Molecular pathways of silica nanoparticle formation and biosilicification. PhD Thesis, University of Leeds, Leeds, UK.

Walter MR, Bauld J, Brock TD (1972) Siliceous algal and bacterial stromatolites in hot spring and geyser effluents of Yellowstone National Park. *Science* **178**, 402–405.